POLITECNICO DI TORINO

Master's Degree in Electronic Engineering

Master's Degree Thesis

Optimization of a clinical Pulse Wave Velocity estimation system based on innovative graphene pressure sensors

Supervisors

Prof. Danilo Demarchi

Ph.D. Alessandro Sanginario

Ph.D. Irene Buraioli

Candidate

Camilla Franchini

April 2023

Abstract

As the World Health Organization estimates, around 18 million of people die from Cardiovascular Diseases every year, making them the leading cause of mortality globally. Early CVD diagnosis and treatment can significantly minimize the risk of premature death and ensure patients a normal life. Among the several potential predictors, arterial stiffness has been shown to be a valuable indicator for assessing cardiovascular risk and is closely related to Pulse Wave Velocity (PWV). The term "Pulse Wave Velocity" refers to the rate at which the pressure wave within the arteries propagates, and it is typically assessed between the carotid and femoral sites. Nowadays, its estimation is executed using expensive technologies such as applanation tonometry and ultrasound, which constrain its usage in a clinical setting and increased over the last few years, the need for non-invasive, low-cost, clinical devices.

For this reason, this thesis project aims to optimize an already designed, at the early experimental stage, clinical PWV estimation system. It is based on a Pyboard D-series and the sensitive elements involved in the transduction mechanism are innovative piezoresistive graphene-based pressure sensors, created in partnership with the Nanochemistry research group, at "Institut de Science et d'Ingénierie Supramolécularies" of the University of Strasburg.

The first part of the thesis has been focused on the characterization of several newly fabricated sensors, with two different shapes: rectangular and circular. They are characterized by a high sensibility and a short time response, which make them a good solution for this application. However, the characterization was a fundamental step to identify and integrate the best functioning one in the system. Then, to consolidate the validation process the system has been tested in a clinical environment, thanks to the collaboration with "A.O.U. Città della Salute e della Scienza di Torino". The results have been inconsistent, revealing a system able to acquire the signal but not giving the stability needed for the application.

For these reasons the second part of the thesis work has been focused on developing a new system configuration to obtain electrical stability and reduce power

consumption; the Pyboard D-series has been replaced with a STM32 Discovery kit, produced by STMicroelectronics. The conditioning circuit, based on a current controlled Wheatstone bridge, has been implemented on two different Printed Circuit boards (PCB). With the goal of reducing the possible noise, each of them has been designed with a specific shape to favour the close integration with the microcontroller board and the sensitive parts.

Given the hardware, a specific firmware has been implemented enabling the acquisition and data transmission to the PC. Among the different aspects that the firmware manages, there is the interaction with the Graphical User Interface (GUI) whose primary purpose is the real-time display of the acquired signals.

Finally, the newly configured system demonstrated its functioning as being capable of acquiring signals and transmitting them via USB to the PC. Compared with the previous, it shows electrical robustness and better performance representing a solid starting point for future optimizations.

Table of Contents

List of Tables VIII

List of Figures IX

Acronyms XIII

1 Introduction 1

2 Background 3
2.1 Physiology of Cardiovascular System . . . 3
2.1.1 Heart . . . 4
2.1.2 Blood Vessels . . . 7
2.1.3 Blood . . . 10
2.2 Cardiovascular Diseases . . . 13
2.2.1 Arterial hypertension and stiffness . . . 16
2.3 Arterial Pulse . . . 17
2.3.1 Morphology . . . 18
2.3.2 Collecting site . . . 19
2.4 Pulse Wave Velocity . . . 20
2.4.1 Clinical devices for PWV estimation . . . 22
2.5 Utilized software . . . 24

3 Piezoresistive Graphene Pressure Sensors 26
3.1 Sensors overview . . . 26
3.2 Sensors characterization . . . 28
3.2.1 Rectangular pressure sensor . . . 29
3.2.2 Circular pressure sensor . . . 33

4 System architecture 37
4.1 Signal conditioning circuit . . . 37
4.2 Initial configuration based on Pyboard D-series . . . 43

4.2.1 Support Design 44
4.3 Signal acquisition limits 47
4.4 Final configuration based on STM32Discovery Board 49
4.4.1 Signal conditioning circuit optimization 49
4.4.2 Discovery Kit STM32F429I 50
4.4.3 Printed Circuit Board design 53

5 Software Implementation 56
5.1 Firmware development 56
5.1.1 Bridge Balancing Algorithm 62
5.2 Graphical User Interface optimization 65

6 Result and discussion 68
6.1 Signal acquisition 68
6.1.1 Rectangular configuration 69
6.1.2 Circular configuration 70
6.1.3 Matlab Analysis 71
6.2 PCB testing 71
6.2.1 DAC102S085 test 72
6.2.2 Voltage reference test 74
6.2.3 INA333 test 75
6.2.4 Programmable Gain Amplifier test 75
6.2.5 Conclusion 78

7 Conclusions and future work 79

List of Tables

3.1 Slope of the characterization curve for rectangular sensors. 31
3.2 Slope of the characterization curve for circular sensors. 35

4.1 Resistance and respective gain values used in the programmable amplifier. 42
4.2 Discovery board GPIOs configured for the implementation of the PGA. 53

6.1 DAC102S08 inspected voltage values on the rectangular PCB. . . . 73
6.2 Analog voltage values measured at the input of the carotid MAX4781 digital switch. 76
6.3 Analog voltage values measured at the input of the femoral MAX4781 digital switch. 76

List of Figures

2.1 Anatomy of the Cardiovascular System, [1]. 4
2.2 Anatomy of the Human Heart, [2]. 5
2.3 The phases of the cardiac cycle, [3]. 6
2.4 Heart's electrical cicle. 7
2.5 Structure of blood vessel 10
2.6 Atherosclerosis. [6]. 14
2.7 Odds ratios for cardiovascular risk factors in the INTERHEART and INTERSTROKE studies [10]. 15
2.8 BP changes depending on endothelium, smooth muscle (SMCs), and extra-cellular (ECs) cells associated with possible hypertensive modifications [14]. 17
2.9 Characteristic notch and peak of the arterial pulse waveform. 19
2.10 Change in the arterial pulse morphology from central to peripheral arteries, [17]. 20
2.11 Pulse Wave Estimation commercial devices. 23
2.12 ATHOS system illustration, [23] 23

3.1 Illustration of the graphene pressur sensor fabrication process, [35] . 27
3.2 Second generation of rectangular graphene pressure sensor. 28
3.3 Second generation of rectangular graphene pressure sensor. 28
3.4 Illustration of the first test setups. Figure 4.8a shows the first setup while 4.8c and 4.8b shows the second setup. 29
3.5 Static resistance evaluation of each rectangular-shaped sensor and its correspondent standard deviation. 30
3.6 Comparison between a not usable and a well usable load/unload cycle of sensor 1 and 10. 32
3.7 Illustration of the two different setup exploited during circular sensors characterization. 33
3.8 Static resistance evaluation of each circular-shaped sensor and its corresponding standard deviation. 34
3.9 Weight loaded sensor during constant weight characterization. . . . 34

3.10 Comparison between a not usable and a well usable load/unload cycle of sensor 1 and 10. 36

4.1 Signal conditioning circuit main stages. 37
4.2 Voltage reference circuit. 38
4.3 Current-based Wheatstone bridge, [41]. 39
4.4 Current reading circuit. 40
4.5 MicroPower Rail-to-Rail Operational Amplifier 4347 pin out description, [46]. 41
4.6 Architectural diagram of the system configuration based on Pyboard D-series SF2W. 43
4.7 3D rectangular designed support for the sensor. 45
4.8 3D pen-shaped configuration designed for the circular sensor. 46
4.9 Pulse Wave Signal acquired at the carotid site plotted on Matlab to investigate the behaviour of the sensor. 48
4.10 Pulse Wave Signal acquired at the femoral site plotted on Matlab to investigate the behaviour of the sensor. 48
4.11 New voltage reference circuit configuration. 50
4.12 Illustration of STM32F429I-DISC1 board. 50
4.13 Input Shift Register of DAC102S085, [48]. 52
4.14 Serial Timing Diagram of DAC102S085, [48]. 52
4.15 Rectangular(a) and Circular(b) sensor-pcb configurations. 53
4.16 PCB layout of the bottom layer. 54
4.17 CAD illustration of the shield configuration obtained integrating the PCB on the Discovery board through specific female header connectors. 55

5.1 Firmware flow chart illustration. 57
5.2 USB buffer structure illustartion. 59
5.3 Firmware flow chart illustration. 62
5.4 Bridge Balancing algorithm flowchart. 64
5.5 Graphical User Interface with a toolbar overview illustration. 65
5.6 Graphical User Interface data reorganization. 67

6.1 Final device configuration based on STM32Discovery Board. 68
6.2 Real time display of the generated signal. 69
6.3 Real-time display of the last signal acquired with the rectangular configuration. 70
6.4 Real-time display of the last signal acquired with the circular configuration. 71
6.5 Rectangular configuration last signal analyzed on Matlab. 72
6.6 Circular configuration last signal analyzed on Matlab. 72

6.7 Voltage values measured on the Carotid PCB. 74
6.8 Voltage values measured on the Femoral PCB. 74
6.9 INA333 output voltage values measured on the Carotid PCB. . . . 77
6.10 INA333 output voltage values measured on the Femoral PCB. . . . 77

Acronyms

CVD
Cardiovascular disease

PWV
Pulse Wave Velocity

DP
Diastolic Pressure

SP
Systolic Pressure

SA
Sinoatrial

AV
Atrioventricular

SBP
Systolic Blood Pressure

DBP
Diastolic Blood Pressure

PWSP
Pulse Wave Systolic Peak

PWdP
Pulse Wave Diastolic Peak

PWD

Pulse Wave Distance

PTT

Pulse Transit Time

ECG

Electrocardiogram

cf-PWV

Carotid-Femoral PWV

GO

Graphene Oxide

ITO-PET

Indium Tin Oxide-Polyethylene Terephtalate

PCB

Printed Circuit Board

IC

Integrated circuits

ADC

Analog-to-digital converter

USB

Universal serial bus

SPI

Serial Peripheral Interface

DAC

Digital-to-analog converter

CMOS

Complementary Metal Oxide Semiconductor

GPIO

General Purpose Input Output

GUI

Graphical User Interface

MCU

Microcontroller unit

SCLK

Serial Clock

CS

Chips Select

MOSI

Master Out Slave In

MISO

Master In Slave Out

CPHA

Clock Phase

CPOL

Clock Polarity

Chapter 1

Introduction

Cardiovascular Disease belongs to a category of disorders related to the heart and blood vessels such as heart failure, hypertensive heart disease, rheumatic heart disease or cardiomyopathy. According to the World Health Organization's estimation, around 18 million people die from CVDs every year. Starting from the 20th century, CVD rapidly diffuses becoming the largest single contributor to global mortality. Given its rapid spreading, extensive research was started regarding the possible risk factor contributing to the disease's development. Among them, arterial stiffness has been proven to be an effective marker for evaluating cardiovascular risk and possibly lowering the chance of developing CVD-related issues. In turn, the most reliable index of hypertensive aortic stiffness is the Pulse Wave Velocity, which represents the propagation speed of the arterial pulse within the arteries. Nowadays is recognized as the leading marker of Arterial Stiffness since the propagation velocity of the wave is strictly related to the elastic and mechanical properties of the vessel's wall.

The currently used technologies for Pulse Wave Velocity assessment are based on non-invasive techniques such as applanation tonometry. Despite their therapeutic relevance, their usage in the clinical setting results to be limited because of the cost. Indeed, according to the European Society of Cardiology, the burden of CVD is not only a health issue but an enormous economic challenge to healthcare systems in the EU, which is expected to grow in future years, [1]. As recent data estimates, Cardiovascular Diseases cost approximately €210 billion a year to the EU economy. Of that, the healthcare cost only accounts for almost 53% (€111 billion).

Therefore, this thesis project aims to optimize an already developed, at the early experimental stage, low-cost and non-invasive Pulse Wave Velocity estimation system based on innovative graphene pressure sensors.

In the first part of the thesis, a discussion on the physiology of the cardiovascular system is provided, followed by a description of the Pulse Wave Velocity and the devices used in the clinical setting to assess it.

The following chapter 3, is entirely dedicated to the active technology. The innovative graphene pressure sensors have been developed by The Nanochemistry research group, at "Institut de Science et d'Ingénierie Supramolécularies" of the University of Strasburg to fabricate a radically new piezoresistive pressure sensor, specific for health monitoring applications. Firstly, an overview of their fabrication process and type is given. Thereafter it is detailed the characterization procedure and the obtained results, carried out to identify the most suitable sensor to be integrated into the PWV estimation system.

After that, the system architecture is presented in chapter 4. Starting from the initial configuration based on Pyboard D-series SFW2, the first optimizations carried out at the device level are described. Then, the new hardware solution based on STM32Discovery board is presented and motivated by the Pulse Wave Signal acquisition limits. After a general description of the STM32Discovery board and its main feature exploited for the system implementation, the focus is on the software implementation.

In fact, in chapter 5, the developed firmware that enables the acquisition and transmission of pulse wave signal to the PC is detailed, together with the adapted Graphical User Interface for their real-time display.

Finally, the device is tested in a non-clinical environment, using the new system configuration consisting of two rectangular graphene pressure sensors and the STM32Discovery board. The obtained results are detailed in the last chapter of this thesis dissertation.

Chapter 2

Background

This chapter provides a physiological background on the cardiovascular system, as well as the concepts of Arterial Pulse and Pulse Wave Velocity. Than, an overview of the existing PWV estimation systems on the market is presented. Lastly, a brief summary of the software utilized throughout the project is provided.

2.1 Physiology of Cardiovascular System

The cardiovascular system is defined as a closed set of vessels called arteries, veins, and capillaries through which the blood circulates under the pumping action of the heart. The system consists of two circulations: pulmonary circulation, which moves blood between the heart and the lungs, and systemic circulation, which moves blood between the heart and the rest of the body. More specifically, systemic arteries provide blood rich in oxygen to the body's tissues then blood returns to the heart through systemic veins, lacking in oxygen. Both circulations are provided with a dense network of capillaries, where nutrients and gasses exchanges happen. As a matter of fact, the complex cardiovascular mechanism plays a crucial role in a human individual life since it guarantees the maintenance of homeostasis. Moreover, with its millions of capillaries permeating every tissue, is capable to reach every cell in the body and feed it with the needed nutrients.
Figure 2.2 shows a simplified scheme of blood circulation for the cardiovascular system where the three key components that guarantee the blood flow are:

- *Blood*: a specialized form of fluid connective tissue consisting of suspended cells in a intracellular matrix, called plasma.
- *Blood Vessel*: channels through which the blood circulate in the body.
- *Heart*: a striated muscular pump for the propulsion of blood in the circular system.

In the next sections, each of them will be presented in more detail.

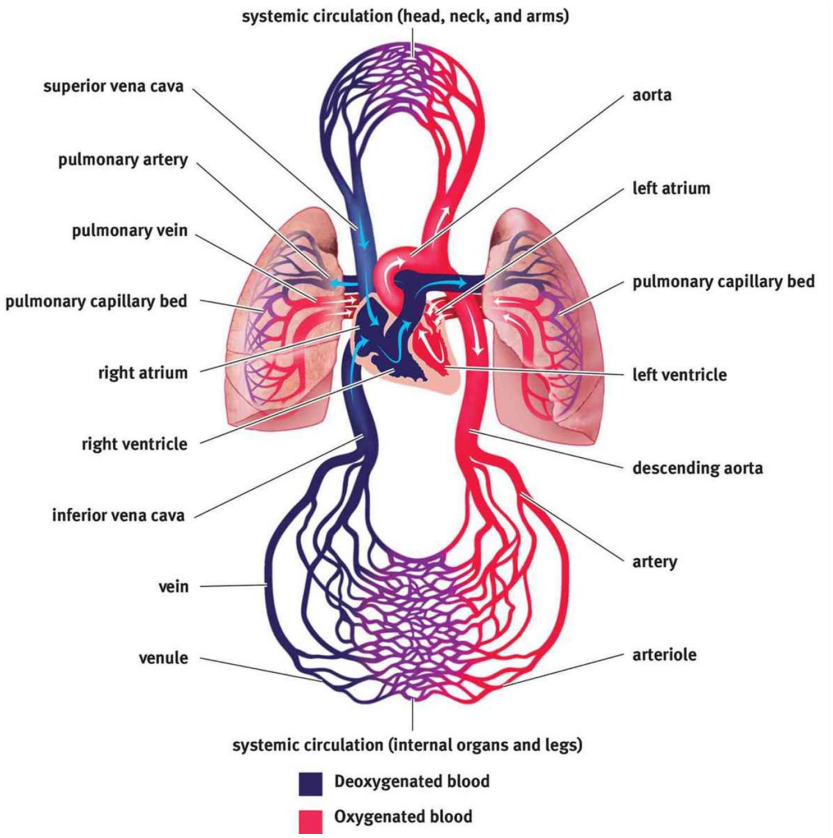

Figure 2.1: Anatomy of the Cardiovascular System, [1].

2.1.1 Heart

The heart represents a primary organ of the circulatory system. It's a striated muscle organ located at the center of the thoracic cavity. It is surrounded by the pericardium, a fluid-fill sac, that has the main fundamental function of lubrication to reduce the friction between the muscle and the surrounding tissues. The heart is mainly composed by cardiac muscle named *miocardium* and its anatomy consist of four chambers: two atria, positioned in the upper part and two ventricle, positioned in the lower. Both atria and ventricles are internally separated by a septum. Specifically the *interatrial septum* for the former while the *interventricular septum* for the latter. Each couple atrium-ventricle, is responsible for a specific circulation: the right side operates the **pulmonary circulation** while the left side the **systemic circulation**. In particular, the pulmonary circuit, is engaged for the transport of deoxygenated blood to the lungs while systemic circuit, transport oxygenated

blood toward all the body's tissues. Therefore, it is fundamental to maintain the correct unidirectionality of blood flow through the heart. This is guaranteed by four valves: two *atrioventricular valves*, the tricuspid and the mitral and two *semilunar valves*, the pumonary and the aortic. Atrioventricular valves, are placed between the atria and the ventricles, preventing the reflux of blood into the atrium when the ventricle contracts. The two semilunar valves instead, are located between the ventricle and the major arteries, preventing the reflux of blood into the ventricle when they relax.

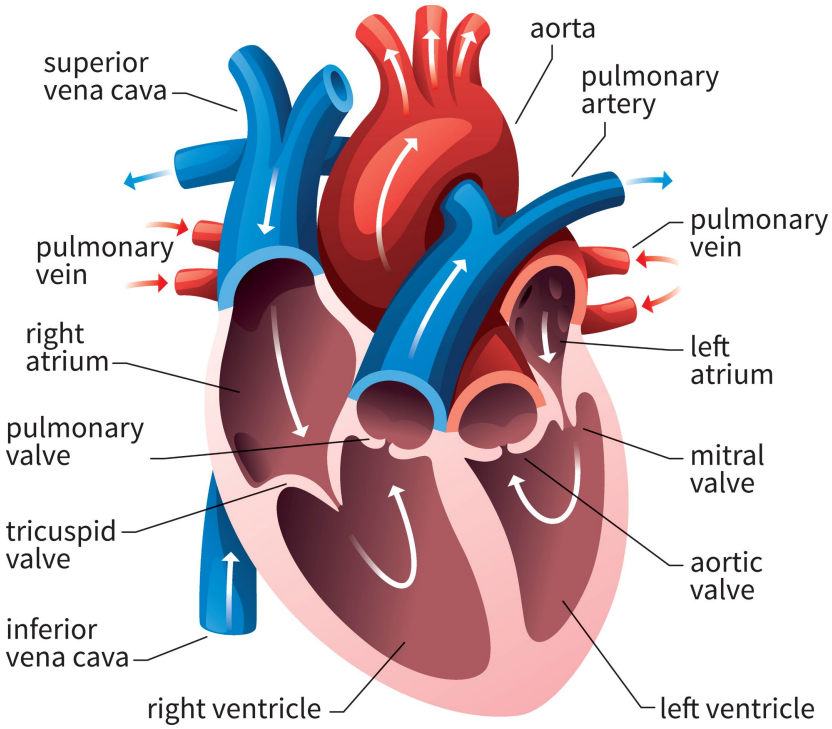

Figure 2.2: Anatomy of the Human Heart, [2].

The cardiac cycle, is defined as the period of time that starts with the contraction of the atria and ends with the ventricular relaxation. It consist in a series of synchronized electrical and mechanical events that guarantee the flowing of the blood inside the circulatory system. The electrical events are related to the depolarization wave and in turn are associated to the mechanical events of the heart, like contraction and relaxation. Indeed, the cardiac cycle, can be divided into two main phases: *diastole*, known as a period of relaxation for the ventricle, and *systole*, known as a period of contraction. Figure represents the entire cycle with its different specific phase. As evidence, the duration of systole is not equal, but less, with respect to that of the diastole. This is crucial for the efficiency of

the heart functioning, indeed a longer duration of diastole allows the prevention of muscle fatigue giving the heart more time to relax. Given that, it is possible to define the diastolic pressure (DP) as the lowest point of the aortic pressure while the systolic pressure (SP) as the maximum.

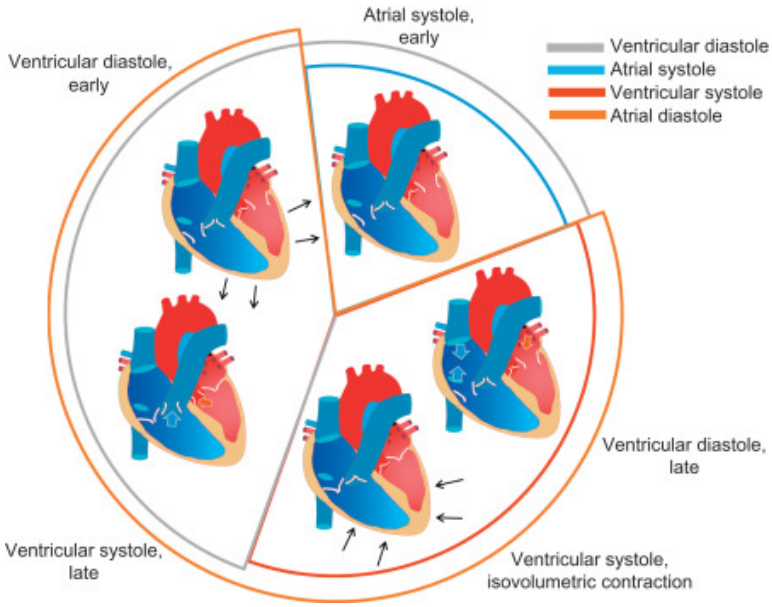

Figure 2.3: The phases of the cardiac cycle, [3].

In the cardiac muscle, there can be distinguished two type of myocardial cells: the *contractile* and the *conducting*. Most of the organ consists of myocardial contractile cells, capable of heart contractions and consequently blood pumping. However, the reaming 1% of myocardial conducting cell has a particular and unique ability to generate an action potential that spreads from cell to cell and trigger the contractile mechanism. This property is known as **autorhytmicity** and grant to the heart the ability to contract without external stimuli. Therefore, the signal for the contraction doesn't come from the nervous system but from these specialized myocardial cell, named *autorythmic*. As a matter of fact, the heart functioning is dictated by electrical signals and their action converge in the so called **heart electrical conduction system**.

Figure 2.4 reports its functioning mechanism; the heart electrical conduction, starts in the *sinoatrial node* (SA), where a single autorythmic cells generates an electrical potential. This electrical stimuli, rapidly propagates to the adjacent cell and give rise to the first depolarization wave. This wave, in turn, while travelling through the *internodal pathway* to reach the *atriovanticular node* (AV), depolarize the atria. From this point, the conduction pathway continues down via the the boundle of His and the Purkinje fibres. By this way, the depolarization continues to propagate up to the upper part of the ventricles allowing to pump blood into the arteries.

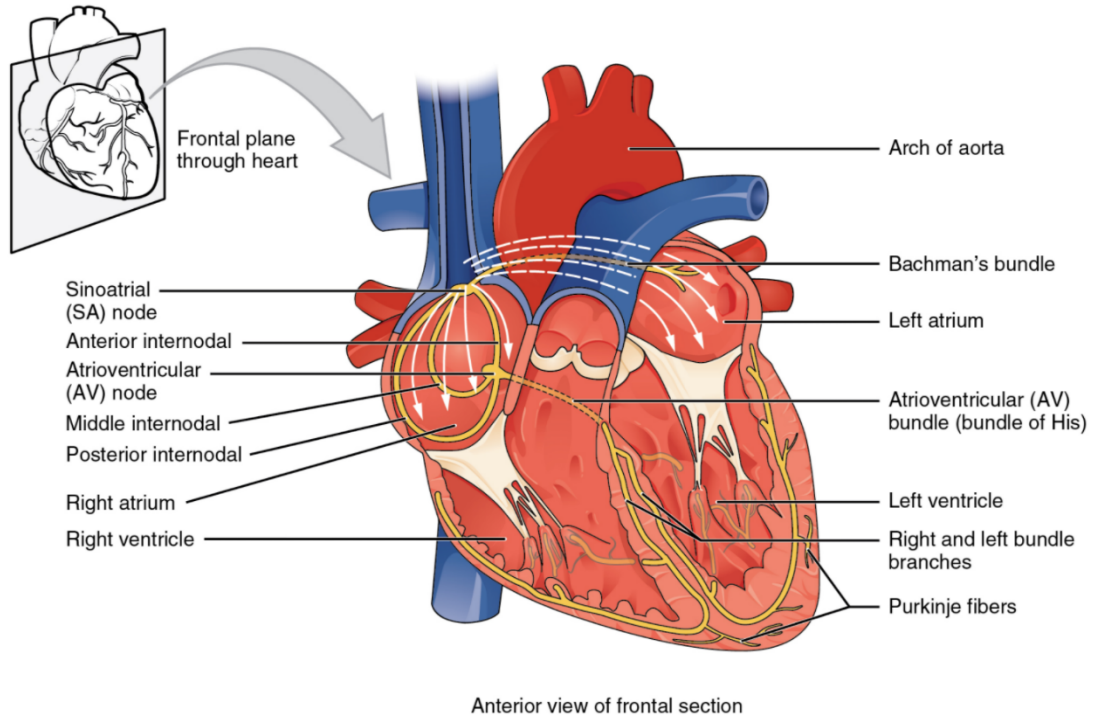

Figure 2.4: Heart's electrical cicle.

2.1.2 Blood Vessels

Perfused by the pumping function of the heart, blood vessels are the elastic conduits of the cardiovascular system and include three fundamental components: arteries, veins, and the microcirculation (arterioles, capillaries, and venules), [4].
Every blood vessel wall's is composed by smooth muscular tissue, fibrous and elastic connective tissue. The presence of elastin guarantees high elastic resistance to the walls, which can contract and release depending on the pressure inside. Collagen,

on the other hand, allows the tissue to lie down without tearing. Vessel's wall presents also an internal coat, called *endothelium*, which has an important role in regulating blood pressure and the transport of nutrient substances.
In the blood vessel structure there can be distinguished three main layer of tissue, from the inside out, they are:

- *tunica intima:* linied by epithelial and composed of connective tissue layers.
- *tunica media:* is the thickest layer of the artery. It is made up of layers of smooth muscle that are held together by connective tissue. This latter is composed primarily of elastic fibers, the majority of which are organized in circular sheets.
- *tunica externa:* substantially made up of connective tissue is composed of collagenous fibers. The outer layers of the tunica externa combines with the surrounding connective tissue and this helps to hold the vessel in relative position.

Blood vessels can be classified according to their size but they share the same general composition, for this reason arteries and veins results in a similar structure. Blood vessel presents a cavity, called *lumen*, through which blood flows. Arteries have smaller lumens than veins, this characteristic is fundamental since ensure the continuity of blood flow through the system even when the heart do not contracts. In comparison to vein lumens, artery lumens appear more rounded in cross section due to their combination of thicker walls and smaller diameters.

Arteries

Arteries are vessels responsible for conducting blood away from the heart. Arteries close to the heart are called *elastic artery* and are characterized by a vessel diameter of around 10 mm. The aorta, which is the one with the largest calibre among all, has a diameter of 12.5 mm and a wall thickness of 2 mm. These thick walls, contain a high percentage of elastic fibers in all the three tunics, infact they should be able to withstand the high pressure of ejected blood. The elastin fibres of the tissue behave like springs, which store energy during the systole and release it during the diastole, pushing forward the previously accumulated blood. Therefor arteries, enables the continuous blood flow because they are capable of expand and contract with the amount of pressure change. This behaviour is scientifically recognized as the blood vessels **compliance**:

$$Compliance = \frac{\Delta V}{\Delta(P_{int} - P_{ext})} \tag{2.1}$$

Where ΔV is the pressure change, while $\Delta(P_{int} - P_{ext})$ is the difference between the internal and the external pressure. When the pressure inside the vessel is lower than the pressure outside, a force directed outwards acts on the wall and promotes its expansion. On the contrary, when the pressure inside is lower, a force is created directed towards the inside, which favours the reduction of volume. According to 2.1 arteries are low complicity vessel which means that a small increase in volume causes a modes expansion accompanied by a high variation in pressure.

Veins

Veins are vessels capable of conducting blood toward the heart. Differently from arteries,they present thin wall and larger irregular lumens. Typical diameter is of 5 mm while thickness is 0.5 mm. The largest veins, such as vena cava, are up to 30 mm in size. Since they are low-pressure vessels, they are supplied by unidirectional valves that allows the flow of the blood only toward the heart, thus avoiding its reflux to tissues. Physiologically veins, are characterized by a greater compliance than arteries, being able to collect larger volumes of blood under the same pressure conditions. As reported in literature, veins contain around 64% of blood volume at any given time and for this reason, can be considered as blood reservoirs. This is possible thanks to their larger lumens and thin walls, that makes them far more distensible then arteries.

Microcirculation

Microcirculation is the terminal vascular network of the systemic circulation consisting of microvessels with diameters lower than 20 µm [5]. Is the last destination of the circulatory system in charge of oxygen transmission from capillary erythrocytes to tissue cells. It is formed by:

- *Arterioles:* they belong to the microcirculation because of their small dimension. In particular, arterioles present a lumen of around 30 µm or less and the thickness of the tunica greatly diminished. The composition of the three layers of tunica slightly change with respect to the larger vessels; it consists of less elastic tissue but more of a smooth muscular one. These muscle fiber, provides arteriole contraction thus changing their diameter and as a consequence the resistance to the flow. For this reason, arterioles have to be considered the primary site of both resistance and regulation of blood pressure.

- *Capillaries:* they are microscopic channels responsible for tissue's profusion of blood. Their diameter ranges from 5-10 µm and their wall consists only of a

thin layer of endothelial cells and a basal membrane. Capillary action consists of the exchange of nutrients and gases between blood and surrounding tissues.

- *Venules:* The capillary network converges to generate venules, which are extremely small capillaries with diameters ranging from 8 to 100 um. They, as well as capillaries, are the principal sites of cell and substance interaction. Veins are formed when many venules unite together.

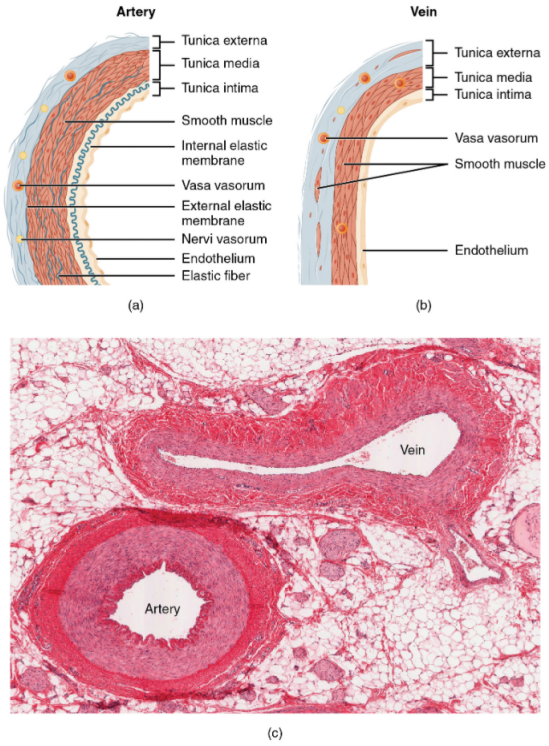

Figure 2.5: Structure of blood vessel
(a) Arteries (b) veins. They have the same general characteristics, but artery walls are significantly thicker due to the higher blood pressure that flows through them. (c) A microscope illustrates the relative thickness difference. [6].

2.1.3 Blood

Blood is a life-maintaining fluid which constantly circulates along the human body providing tissues and organs with nutrition, oxygen, and waste removal.
It is classified as connective tissue since it is made up of similarly specialized cells that serve particular functions. Yet, these cells are suspended in a liquid matrix known as plasma, which causes blood to be fluid. Blood has an extremely

complicated composition, however on average, it contains two distinct phases: a liquid phase, the **plasma**, and a solid phase also called **figurative elements** since it is formed by cells and cell-derived components.

Plasma

Is the slightly yellowish liquid making up about 54% of the blood volume. It is a complex solution containing more than 90%of water together with sugar, lipids, proteins and other important nutrients. More specifically, plasma differs from extracellular fluid of the tissues for its high protein content. As matter of facts, the major solute of plasma is a heterogeneous group of proteins. The predominant plasma protein is serum albumin, a tiny molecule whose main function is to retain water in the bloodstream via an osmotic action. The overall volume of plasma is determined by the amount of serum albumin in the blood. Depletion of serum albumin permits fluid to leave the circulation and to accumulate and cause swelling of soft tissues (edema) [7].

Figurative Elements

The figurative elements constitute 45% of the blood volume of a human individual, with a slight variation depending on whether is a male or female. The characteristic opaque red colour is imparted by haemoglobin, an iron-containing protein. Haemoglobin brightens in colour when saturated with oxygen and darkens when oxygen is removed [7]. In the solid phase, there can be distinguished three main blood cells, each of them with a specialized function:

1. **Erythrocytes**: or red blood cells, they are the most numerous figurative elements. With an average of around 5.000.000 for mm^3 they are anucleate and characterized by a biconcave disc form. The typical diameter size is around 7-8 µm while their particular shape facilitates faster oxygen diffusion in the cell. Erythrocyte's main function is to take up oxygen from the lungs and distribute it to tissues.

2. **Leukocytes**: or white blood cells, they have a fundamental defence role and for this reason, are involved in the immune system. They comprise three different cell classes: granulocytes, monocytes and lymphocytes. Specifically, they are responsible for the destruction of infected agents and the secretion of substances such as antibodies. Leukocytes use the circulatory system to reach the different parts of the body.

3. **Platelets**: consists in the smallest blood cell, with a disc form of a 2-3 µm diameter. Their presence, in number, ranges between 150.000 to 440.000 for

μL. They form in the bone marrow by segmentation of the cytoplasm and then are released into the bloodstream. Here, platelets are involved in the fundamental survival process of blood clotting. More specifically, their main function refers to the homeostasis mechanism. When the surface of a blood vessel is injured, they immediately attach in large numbers and form a solid, resistant mass of platelets.

Blood Pressure

According to its definition, blood pressure refers to the force exerted by the blood against the vessel's wall when pumped by the heart. More specifically, blood flows through arteries and veins as a function of ventricular contraction.
The governing principles of this blood flow and its behaviour in the vessels is well known and described by *Hemodynamics*; the science of the physical and physiological principles governing the movement of blood through the circulatory system. "There can be no true understanding of the circulation without an appreciation and understanding of some basic hemodynamic principles" [8].
The basic law of hemodynamics is the Bulk Flow Law:

$$Q = \frac{\Delta P}{R} \tag{2.2}$$

where ΔP is the intravascular pressure gradient (measured in millimetres of mercury) between the upstream (higher pressure) and downstream (lower pressure) ends of the blood vessel and R is the blood resistance.
According to the formula 2.2, for there to be a flow, it is necessary that a pressure difference occurs between two points standing at a difference pressure level. This generates a gradient and enables the flow of the liquid volume. The flow will be characterized by a rate Q expressed in ml/min, proportional to ΔP and inversely proportional to the resistance to flow, R.
The resistance R is the systemic vascular resistance. It includes all the factors that hinder the flow, including the size and shape of the blood vessel that, being narrower or wider, can alter the ease of blood flow. Resistance in a vessel is described by Poiseuille's low, discovered a century ago during the conduction of experiments involving tubes of various sizes and fluids of different viscosity. The scientist found that resistance R is a function of viscosity h, tube length l, and tube radius r, as described in 2.3:

$$R = \frac{8L\eta}{r^4\pi} \tag{2.3}$$

Poiseuille's equation represents an approximation of reality considering that several constraints and assumption has been imposed for the achievement of its formulation.

Among them are the most important:

1. Flow through the tubes is steady;
2. The vessels are rigid, cylindrical, straight tubes with a uniform shape that is longer than it is wide.
3. The fluid flowing is a Newtonian fluid characterized by a constant viscosity.

As a matter of fact, most of these assumptions results to be violated considering the human cardiovascular system. Indeed, flow in arteries is pulsatile and can be turbulent. Vessels are elastic and compliant, far from being rigid. Blood is not homogeneous but a suspension of cells in plasma. Nevertheless, the value of Poiseuille's equation exists and plays an important role in the revelation of CVDs. As an example, if arterial pressure shows an increase of only 20% and this sustain over time, it might be related to hypertension.
Blood pressure is typically measured in individuals using a specific cuff placed over the brachial artery or the femoral artery. **Systolic pressure** pressure (the greater pressure) is the force of the blood on the artery walls while the heart pumps blood to the peripheral organs and tissues, and **diastolic pressure** (the lower pressure) is the residual pressure exerted on the arteries when the heart relaxes between beats. In clinical practice, blood pressure is calculated as Systolic Pressure (SP) divided by Diastolic Pressure (DP). Systolic pressure is normally around 120 mmHg while Diastolic pressure is 80 mmHg, hence for a young healthy subject the blood pressure should be about 110/70 (SP/DP).

2.2 Cardiovascular Diseases

Cardiovascular diseases represent the category of heart and blood vessel disorders. As the World Health Organization estimates, around 18 million people die from CVDs every year, making them the leading cause of mortality on a global scale. For the past 100 years, the trajectory of cardiovascular diseases has followed the epidemiological transition course and has been in line with global economic development. Individuals, growing up in developed countries were uncommonly subjected to cardiac surgery and possible myocardial infarction but then, starting from the 20th century, CVD rapidly diffuse becoming the largest single contributor to global mortality.

CVD can be considered a general term that identifies a specific condition affecting the cardiovascular system like coronary heart disease, stroke and rheumatic heart disease. However, what unites all these conditions, is the cause. Cardiovascular diseases originate from atherosclerosis. This pathology develops slowly over time, involving the attachment of cholesterol plaque, a fatty material, to the wall of

the blood artery. The presence of the plaque, hardens the blood flow through the artery, creating unwanted blood clots. With the worsening of the condition, clots formed in the artery results into stroke and heart attack.

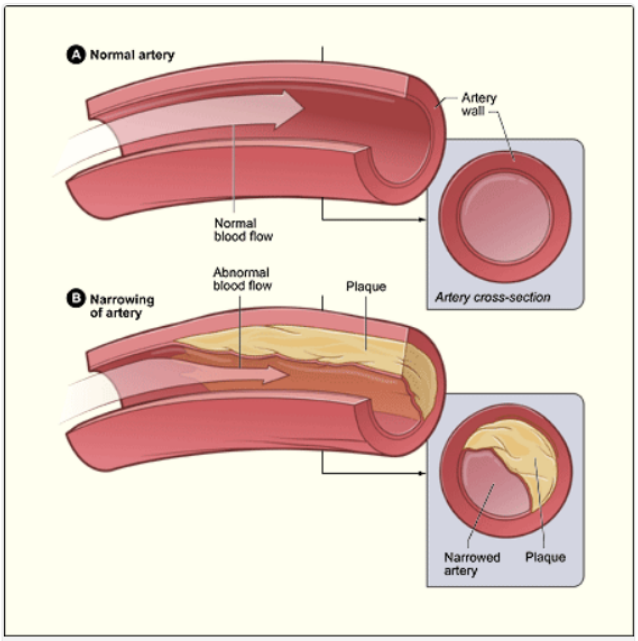

Figure 2.6: Atherosclerosis. [6].

Given the rapid spreading of CVD, starting from the 20th century extensive research regarding the possible variables, contributing to the development of CVDs, i.e risk factors, has been carried out. The precursor has been the Framingham study, launched in 1948 with the original goal of identifying the common factors that contribute to cardiovascular disease. Over the years, the FHS has become a successful, multigenerational study that analyzes family patterns of cardiovascular and other diseases [9], enabling the categorization of the risk factor into two main groups:

- *Behavioural risk factors*, such as tobacco and alcohol use, unhealthy diet and physical inactivity.
- *Metabolic risk factors*, such as raised blood pressure (hypertension), raised blood lipids (e.g. cholesterol), raised blood sugar (diabetes), overweight and obesity.

About that, two recent important case studies have reported an analysis of the role of the major CVD risk factor in determining the risk of myocardial infarction (inter heart study) and stroke (interstroke study). As shown in graph 2.7, nine

easily assessed and traditional risk factors such as Tobacco smoking, hypertension, diabetes, abdominal obesity, and psychosocial factors can be statistically associated with a significantly increased risk of myocardial infarction. On the other hand, an odd ratio below 1 (thick line), reports helpful factors. In particular, daily consumption of fruits and vegetables, regular low to moderate alcohol consumption, and regular physical activities were associated with reduced risk. These associations were present in women and men, old and young, and in all regions of the world

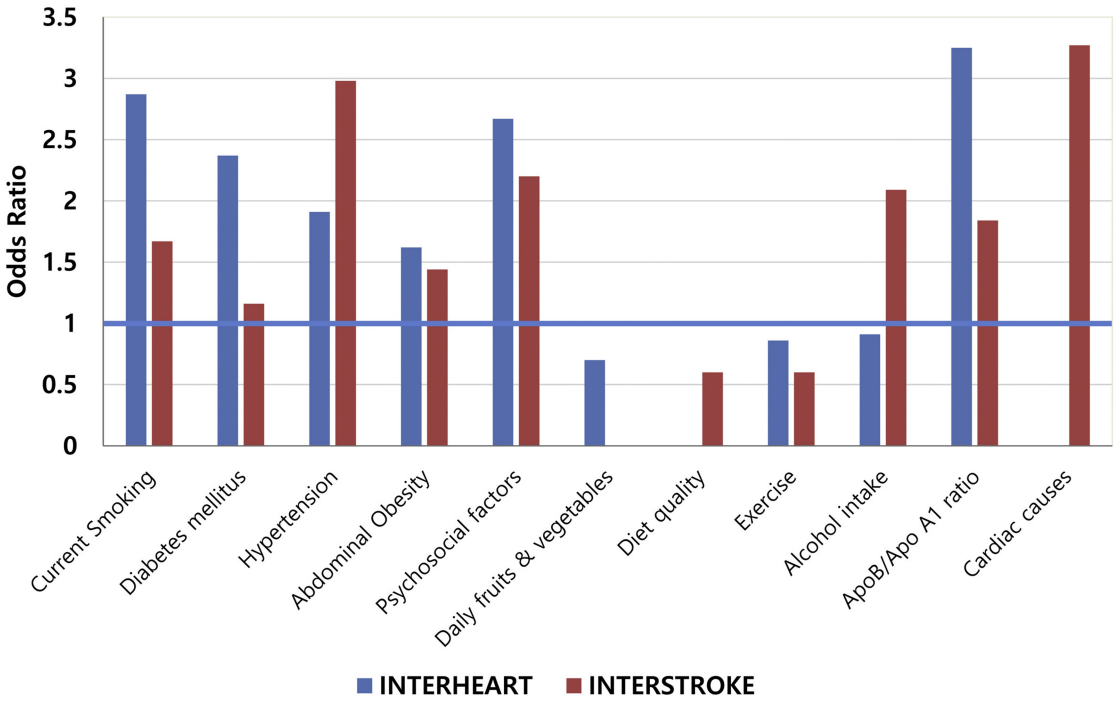

Figure 2.7: Odds ratios for cardiovascular risk factors in the INTERHEART and INTERSTROKE studies [10].

Worth of notice that, among the numerous risk factor reported, Hypertension is associated with the highest risk for stroke, with an ORs of 3.0 or more. In the next section, an in-depth analysis of this and its direct consequence will be presented. At last, it has to be considered the impact of the CVD's global spreading on the economy. In the United States alone, adult-related spending on cardiovascular disease grew by more than 100 billion between 1996 and 2016, totalling about 320 billion each year in direct costs such as inpatient costs, ambulatory costs, expenses for prescribing drugs, nursing care facility costs and expenses for the management of the emergencies [11].

Given that, it is essential to put into practice workable and cost-effective methods for the prevention, early detection, and control of diseases, as well as to monitor the results and reduce premature death due to CVD.

2.2.1 Arterial hypertension and stiffness

Arterial hypertension is responsible for up to 10 million deaths worldwide resulting to be a leading contributor to the global burden of cardiovascular diseases [12]. As a matter of fact, it is one of the main exponents of CVD's risk factor. Although its a high prevalence and a huge impact on global human health, awareness of this disease are typically low, even in affected people. Hypertension is defined also as high blood pressure, indeed it consists in a chronic condition for which systolic blood pressure (SBP) values are higher than 130mmHg and diastolic blood pressure (DBP) more than 80 mmHg. Most cases of hypertension are asymptomatic but its impact on the cardiovascular system is massive. High blood pressure, forces the heart to pump harder in order to maintain a "normal" pressure condition. If from one side, thanks to the elasticity of the smooth muscle building up heart and vessels, this can be tolerated even for years, from the other, the risk of myocardial infarction or a heart attack increases importantly.

Blood pressure monitoring represents the only way for the detection of a hypertension condition. However, for years, several predictive parameters have been discovered to possibly help with early diagnosis and consequently lower the chance of developing hypertension related problems. Among them, arterial stiffness has been revealed as a reliable predictor of cardiovascular risk in patients with essential hypertension. Furthermore, according to studies, it has been marked as an high-priority therapeutic target to ameliorate the global burden of cardiovascular disease [13].

Stiffness is a generic term, representing the relation between stress and strain applied to a specific material, herein the artery walls. A healthy aorta exerts a powerful cushioning function which moderates the flow of the pulsatile pressure towards the periphery and protects the microcirculatory network. Therefore, in a healthy individual, going from the aorta toward the muscular peripheral arteries, it is possible to identify an increasing, heterogeneous, stiffness gradient. This gradient tends to fade with ageing or in pathological conditions such as hypertension. In particular, for this latter condition, the pulsatile pressure transfer to the microcirculation increases, potentially raising the risk of brain, heart, and kidney injury. [14].

To this purpose, studies on hypertension condition demonstrated that in order to avoid increased capillary pressure, adaptive changes in the mechanosensitive function of the vascular endothelium and smooth muscle become necessary. Including a steeper slope of the pressure–arterial diameter relationship, as shown

by the middle curve in 2.8, [14]. Conversely, with increasing age, the amount of elastin in the vessel walls declines throughout the arterial tree, while a material such as a collagen or fibronectin increases. The direct consequence is an increase in arterial stiffening. The most reliable index of hypertensive aortic stiffness is the Pulse Wave Velocity which will be discussed in detail in the next sections.

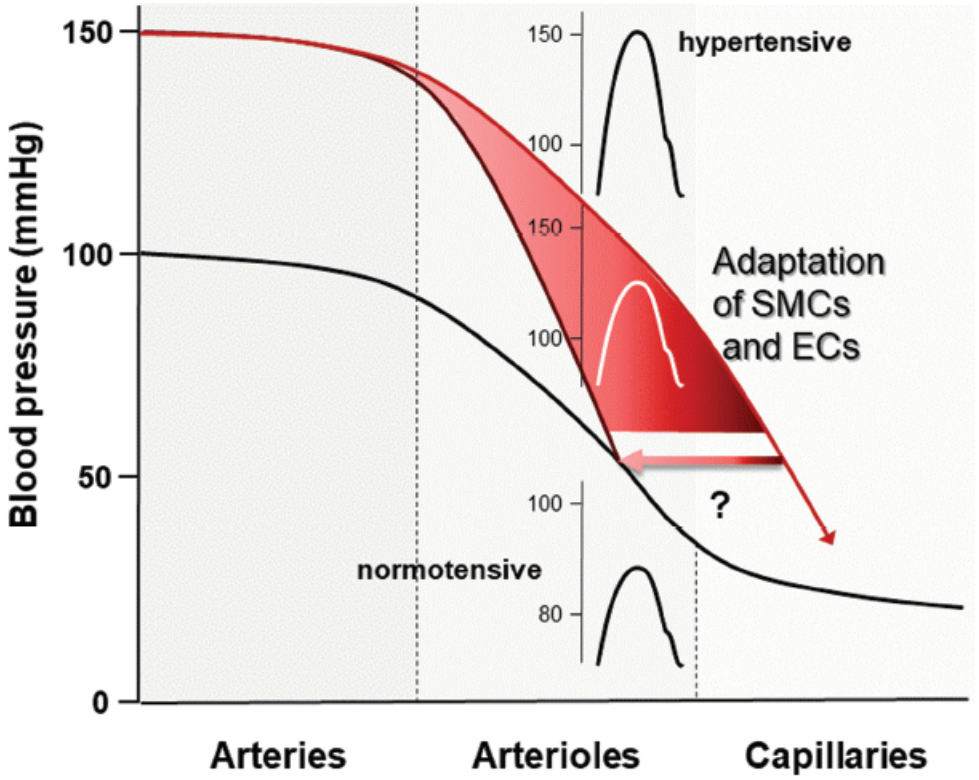

Figure 2.8: BP changes depending on endothelium, smooth muscle (SMCs), and extra-cellular (ECs) cells associated with possible hypertensive modifications [14].

2.3 Arterial Pulse

By definition, the arterial pulse is the abrupt expansion of an artery resulting from the sudden ejection of blood into the aorta and its transmission throughout the arterial system [15].

Arterial pulse refers to the pressure wave, generated by the heart's systole, known as a sphygmic wave. This, thanks to the flexibility of the artery walls, travels

through the peripheral system. The arterial pulse wave can be assessed whenever arteries are closer to the skin surface, thus are perceptible by palpation. The main locations for its determination as a vital sign include radial, brachial, carotid, and apical points while the techniques vary according to the location. Considering that the pulse rate, is synchronized with the heartbeat, the main application of the arterial pulse is the heart rate estimation. However, the estimation of the pulse characteristic has increased over years because of the several important clinical parameters that can be derived by analyzing the signal waveform.

2.3.1 Morphology

Although the shape and width of the arterial pulse wave tend to change as it propagates along the vascular tree, considering the course of a single cardiac cycle, there can be identified some characteristics point describing its morphology. First of all, two distinct phases can be recognized: the systolic phase, corresponding to the anacrotic limb, and the diastolic phase, corresponding to the dicrotic limb. As figure 2.12 shows, the waveform presents two main peaks, Pulse Wave Systolic Peak (PWSP) and Pulse Wave Diastolic Peak (PWDP). The former shows up due to the influence of reflected waves generated into the vascular system and for this reason, it represents the maximum pressure generated during the ventricular ejection, the latter is after the dicrotic notch and is due to the aortic valve elastic rebound, when it closes at the end of the ventricular ejection. The other three important points of changing slope highlighted in the figure as A,B,C, instead, has the following specific meaning:

A. *Systolic upstroke:* it is the sharp rise starting at the aortic root. This positive growth of the wave is generated by the peak of aortic blood flow at the opening of the aortic valve. The slope is related to the pressure variations inside the left ventricle and with the efficiency of the aortic valve, thus a slurred slope possibly highlights aortic stenosis;

B. *Systolic decline:* it is the quick pressure decrees occurring at the end of the systole. It occurs because the efflux of blood from the artery is faster than the influx from the ventricle;

C. *Diastolic runoff:* it is an exponential pressure decline observed after the closure of the aortic valve. As soon as the ventricle stops pumping blood inside the aorta, the pressure decreases progressively. The down stroke of the arterial waveform indicates how much resistance exists throughout the vascular tree to sustain pressure once left ventricular ejection into the arterial tree has stopped, [16]. Therefore, the sharp or shallow decrease of the waveform, the downstroke, is an indication of higher or little resistance to blood flow which allows recognizing possible cases of heart failure.

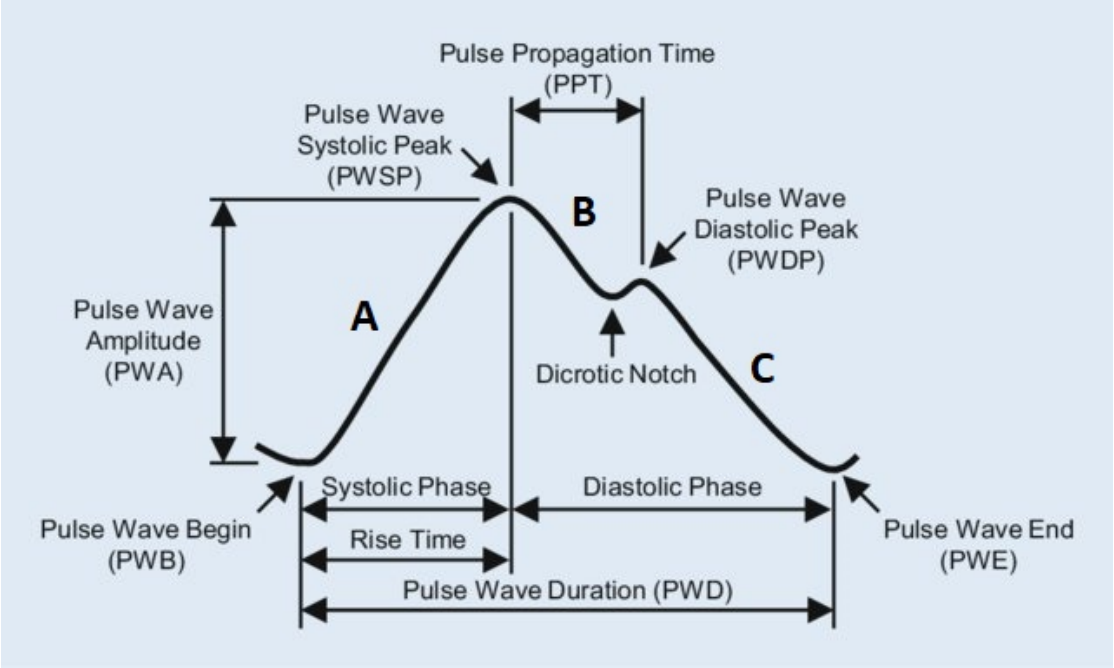

Figure 2.9: Characteristic notch and peak of the arterial pulse waveform.

The pulse waveform provides other several parameters effective for the monitoring of the cardiovascular system condition:

- *Pulse Wave Amplitude(PWA)*: also called systolic amplitude, is given as the difference between the arterial pulse signal's baseline (PWB in figure) and systolic peak pressure (PWSP in figure).
- *Pulse Wave Width*: is given as the interval between the beginning and the end of the pulse. Pulse Wave Width and amplitude, are used as an indicator of the possible hypokinetic or hyperkinetic condition thus suggesting myocardial infraction or severe aortic regurgitation, [15].
- *Area Under The Curve(AUC)*: allows for the calculation of the Mean Arterial Pressure(MAP). MAP is the mean pressure averaged over time in the arterial tree at a defined locus (i.e., aortic arch, abdominal aorta, and radial artery) and is typically an effective indicator of tissue perfusion.

2.3.2 Collecting site

Arterial pulses can be detected at a variety of sites throughout body. These can be classified into central pulses, which are collected close to the heart, and peripheral pulses, which are recorded far from the heart.

Although mean blood pressure decreases from the central aorta to the peripheral arteries, the systolic pressure increases. Therefore, arterial pulse changes as it travels from the central aorta down to the peripheral arteries. The pulse can be distorted and damped as the distance from the heart increases, due to reflected, resonance, or standing waves, as well as changes in the elastic characteristics and calibre of the peripheral arteries in the upper and lower areas of the body. In particular, the amplitude of the pulse increases going far from the heart and the systolic upstroke becomes steeper because of the high resistance of small arteries. The dichroic notch stops being a sharp interruption and instead, gradually declines, a sign of a steadily decreasing pressure value. It also appears increasingly delayed if compered with the systolic peak pressure.

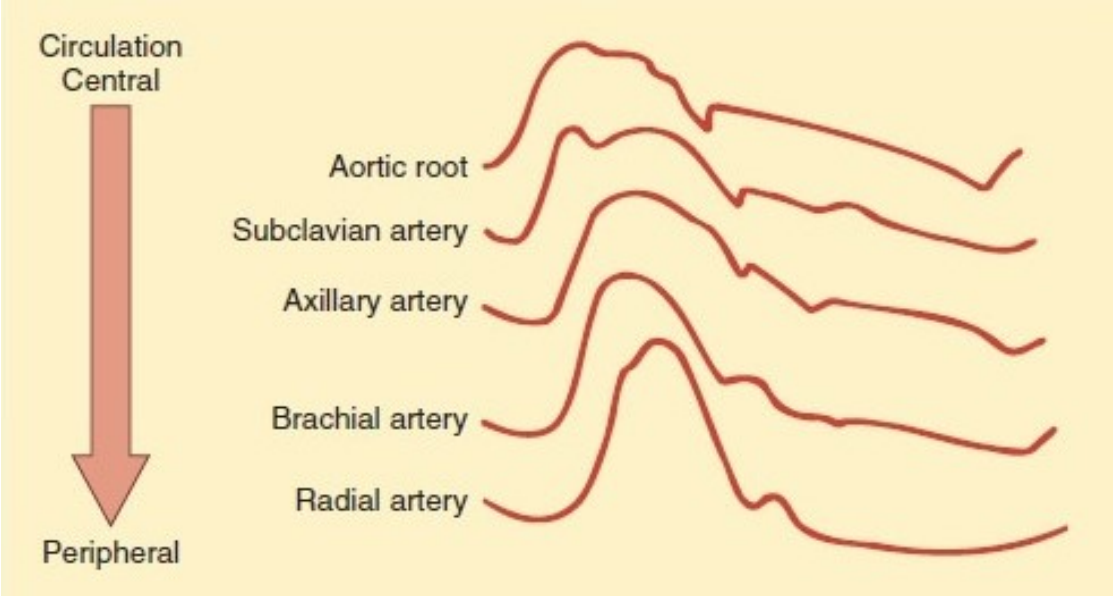

Figure 2.10: Change in the arterial pulse morphology from central to peripheral arteries, [17].

2.4 Pulse Wave Velocity

One increasingly important parameter that can be derived from the pulse wave is the Pulse Wave Velocity. It represents the speed at which the arterial pulse propagates within the arteries [18] and is generated by the systolic contraction of the heart. It is recognized nowadays as a leading marker of Arterial Stiffness [19] since the propagation velocity of the wave is strictly related to the elastic and mechanical properties of the vessel's wall.

Arterial stiffness refers to a mechanical property of the arteries wall and typically, the stiffer the artery the greater the PWV. Thus, in young healthy individuals, the wave propagation speed will results slower than that in older patients because their tunica media has much more prevalent elastic components. Healthy conditions are characterized by Pulse Wave Velocity values of 5 to a maximum of 10 m/s while, for some pathology, these values can reach up to 15 m/s.

The PWV estimation, relay on the measurement of the arterial pressure wave on two specific sites of the arterial tree: a **proximal site** and a **distal site**. As already mentioned in the previous paragraph 2.3.2 several different reference measurement sites are used in clinical practices, however, the gold standard for noninvasive AS measurement is the carotid-femoral PWV (cfPWV), which has been successfully validated as an independent predictor for all-cause mortality and cardiovascular morbidity, [19].

The velocity is obtained as the ratio between the c-f's pathway distance PWD (this distance can be obtained by doing direct measurements or subtracting ones) and the time delay of the pulse wave from the first to the second measurement site, called Pulse Transit Time (PTT). This ratio needs to be multiplied by a scaling factor of 0.8, in order to correct the overestimation of the real velocity.
While the PWD quantity, whether it is direct or indirect, is obtained by the clinician through a measuring tape, the PTT has two possibilities:

- *Two-step method*: requires a single probe but the ECG signal integration. The R peak of the ECG, which is a representation of ventricular ejection, serves as a reference point in this approach, which separates the PTT examination into two parts. The first step consists to extract the carotid PTT (cPTT), which is the time it takes for the blood pulse to travel from the heart to the carotid. Then, the probe is positioned at the femoral site, where the same procedure is executed. Finally, the PTT suitable for the Pulse Wave Velocity estimation is obtained from the difference between the two acquire signals.

- *One-step method*: requires two probes, able to simultaneously record the pulse wave on both the carotid and femoral site thus, enabling a quick assessment of the differential PTT without the need for the ECG signal.

In clinical research, the arterial tree is represented through a " *propagative model"* of viscoelastic tube terminating with peripheral resistance [19]. The Moens-Korteweg is the equation used to calculate the velocity of propagation, PWV, taking into account the E, Young's elastic modulus of the wall, h the wall thickness, ρ the density of the liquid and d the diameter of the tube.

$$PWV^2 = \frac{Eh}{2R\rho} \tag{2.4}$$

Later, the Moense-Korteweg equation was further expanded by Bramwell and Hill that use vascular physiology to describe the correlation between relative changes in volume (ΔV/V) and pressure (ΔP).

$$PWV^2 = \frac{\Delta PV}{\Delta V \rho} \tag{2.5}$$

Furthermore, the variation in volume ΔV, related to the pressure variation ΔP as a function of the initial volume V of the vessel [19] is defined as distensibility. By considering formula 2.4 and substituting in formula 2.5, it is possible to obtain an inverse proportionality between the PWV and distensibility, thus, a direct indicator of arterial stiffness. The greater the PWV the higher the AS.

$$Distensibility = \frac{\Delta V \rho}{\Delta PV} = \frac{1}{PWV^2} \tag{2.6}$$

2.4.1 Clinical devices for PWV estimation

Based on numerous studies and validation trials, the Pulse Wave Velocity is nowadays set as a gold standard for AS determination and consequently for the early detection of possible cardiovascular events. Several various devices have been adopted for their clinical application, with an increasing emphasis over the years on the development of non-invasive devices that mostly perform a regional PWV measurement (across a long arterial segment) rather than local PWV measurement (over a short arterial segment).

The most widespread method for identifying the pressure wave produced by the heart's systolic ejection is applanation tonometry; a technique that relies on the detection of change in the surface tension of the tonometer due to the pressure exerted by the pulse wave.

The main employed commercial devices based on this method are presented in the following:

SphygmoCor® SphygmoCor (AtCor Medical, Sydney, Australia) is considered the golden standard for the cfPWV measurement. The tonometer is mounted on a pen shape support and it executes the measurement of PWV using the two-steps method. For this reason the additional ECG recording is necessary.

Complior® Complior (Colson, France) is equipped with two piezoelectric pressure transducers allowing for the simultaneous detection of the pulse from the carotid and the femoral sites. In this case, there is no need for ECG detection.

PulsePen® The PulsePen (DiaTecne, Milan, Italy) is composed of a tonometer, enclosed into a pocket-sized case, and an ECG unit allowing for the implementation of the two-step method.

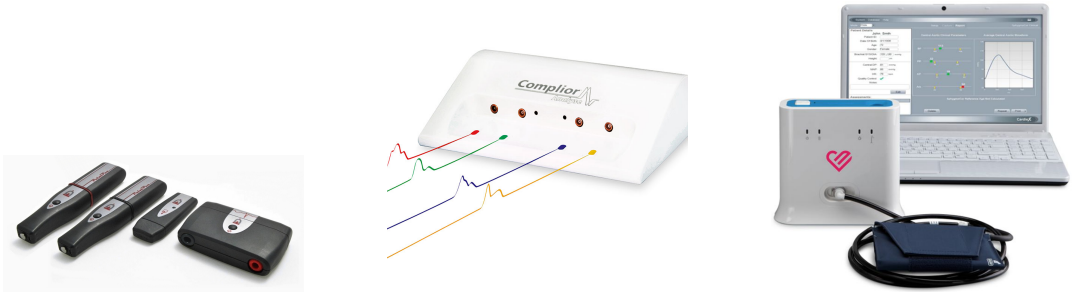

(a) PulsePen device illustration, [20].

(b) Complior device illustration, [21].

(c) SphygmoCor device illustration, [22].

Figure 2.11: Pulse Wave Estimation commercial devices.

Another interesting but non-commercial device based on a tonometer is the ATHOS [23] system. Developed at the "Politecnico di Torino",its sensitive component consists of two MEMS pressure sensor LPS35HW produced by STMicroelectronics. The two tonometers are enclosed into two pen-shaped probes connected to a main unit responsible for signal acquisition. The device exploits the one-step method but can also be equipped with an external electrocardiograph, which therefore allows for two-step measurement [23].

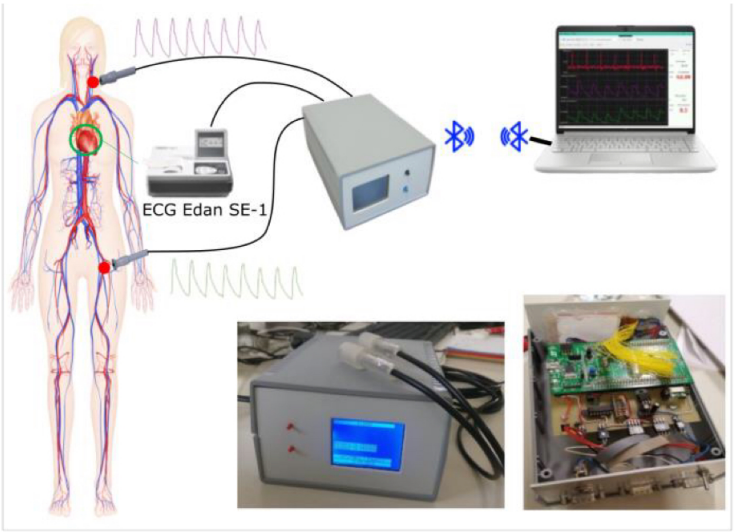

Figure 2.12: ATHOS system illustration, [23]

2.5 Utilized software

The present section describes the software tools used for the thesis project's development:

LabVIEW (Laboratory Virtual Instrumentation Engineering Workbench) is a development environment for the visual programming language of National Instruments, the G language. It is characterized by a graphical syntax used for data collecting and analysis, process control or industrial automation. The data structures and algorithms are made up of icons and other graphic entities, linked together through the use of unidirectional wires to build the so called, flow diagram. In this thesis work, Labview has been used to acquire data directly from the Agilent 34411A multimeter, plot them on a graph and save them in a specified Excel file. In particular, it has been used during the characterization of the graphene pressure sensors to measure their output resistance variations.

SolidWorks is an industry-leading CAD (Computer-Aided Design) software, developed by Dassault Systèmes. It was initially utilized to design the supports needed for the characterization of the pressure sensor, both rectangular and circular in shape. It was then used for the redesign of the sensors' support integrated into the final system. After their design, the 3D models has been printed using a 3D resin printer, the From3.

Pycharm is a Python language integrated development environment (IDE), developed by JetBrains. It was initially used to manage the PWV signal acquisition through the developed Graphical User Interface(GUI).

MATLAB is a MathWorks developed high-level programming language and a numerical computation environment. It supports matrix manipulation and is written in C. It is used for implementing algorithms, evaluating data, and constructing control systems thanks to the many different toolboxes available. For the thesis's aim, it has been utilized for analyzing the acquired PWV data and understanding the signal acquisition issues encountered during the system validation. Furthermore, it has been fundamental to elaborate the result obtained from the sensors characterization.

STM32CubeMX is a graphical utility for easily configuring STM32 microcontrollers and microprocessors. Developers start the project by selecting their board or microcontroller. After that, it is possible to configure the needed peripherals such as ADC, SPI, GPIOs, USART and set up the clock tree. As a result, shifting

from writing C code to using the configuration utility results much easier. In this work, it has been used as starting point for the understanding of the microcontroller and peripherals management.

Keil Vision®5 is a free Integrated Development Environment (IDE) supplied by the ARM Holdings, that combines in a single environment many important features such as project management, runtime environment, source code editing, and program debugging. Thanks to the Software Pack it also offers the possibility to create software applications starting from prebuild examples. In this thesis, it has been widely used for firmware development, written in C language, and its following testing through the debug environment.

Visual Studio 2022 is an integrated development environment (IDE) developed by Microsoft that supports many aspects of software development such as editing, debugging, and building code. This environment has been utilized to optimize and adapt to this work application a graphical user interface written in C# language. The interface allows for the realtime display of the signal from the carotid and femoral sites and to save the corresponding data in a binary file.

Chapter 3

Piezoresistive Graphene Pressure Sensors

In this section, the piezoresistive graphene pressure sensor integrated into the developed system is presented. Together with its fabrication method and the two different developed structure, it will be reported the characterization carried out to identify which is the most suitable sensor for integration in the Pulse Wave Velocity estimation system.

3.1 Sensors overview

A pressure sensor is a device able to produce an output electrical signal as a response to an input applied pressure. The piezoresistivity instead is the technology on which the pressure sensor relay on and refers to the material's property. In particular, if a piezoresistive material is subjected to a certain amount of pressure, it undergoes a strain that will reflect changes in its electrical resistivity (piezoresistive effect). Typical piezoelectric materials are semiconductors, however, over the last years, many other different nanostructured materials, including graphene, have been explored to construct stretchable piezoresistive sensors on an elastomer substrate.

The sensor exploited for this thesis project has been developed by The Nanochemistry research group, at "Institut de Science et d'Ingénierie Supramolécularies" of the University of Strasburg with the aim of fabricating a radically new piezoresistive pressure sensor, specific for health monitoring applications, characterized by a sensitivity as high as 0.82 kPa^{-1}.

To obtain such property, the active part has been realized by reacting commercially available graphene oxide(GO) with amino-functionalized molecules to form covalent bonds on the basal plane of GO, [35]. Then, specific successive fabrication steps, conduct the growth of the molecular pillars perpendicularly to the graphene

plane, yielding a multilayered structure. The obtained conducting ink is spry coated onto a Flexible PCB substrate made of Kapton, capable of significantly reducing the electrical noise due to its intrinsic property of insulation. The two substrates are then fixed facetoface and kept together with Kapton tape. Finally, a tin layer of gold, attached to the extremities of the structure, realizes the electrical contacts. The use of gold drastically influences the baseline resistance value, which is less than 1Ω. When pressure is applied on the surface of the sensor, the molecular pillars become shorter reducing the interlayer distance between the rGO sheets. From an electronic point of view, this involves an increase in the tunnelling current through the layers and a resistance decrease. Thus, the sensitivity of the sensor is significantly improved thanks to the upstanding flexibility of the tri ethylene glycol amine.

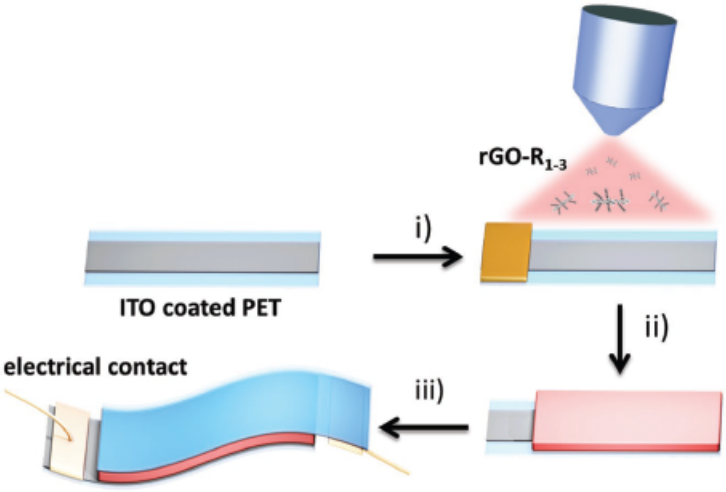

Figure 3.1: Illustration of the graphene pressur sensor fabrication process, [35]

Two different shapes were developed: the rectangular 3.3, whose structure consists of that described in the previous paragraph and the "circular cross" shape. This latter presents a much more complex geometry; it is comprised of two Kapton flexible PCBs that are overlapped plus multiple gold electric lines allowing the current to flow thought the two crosses. According to figure **??**a, the Kapton is exclusively functionalized with GO at sites A, B, C, and D. In this way, each cross's arm functions as a tiny, rectangular sensor where the current stream enters into the IN-point, passes through the four functionalized areas linked by the gold tracks, and exits from the OUT-point. This configuration enables the sensor to be stimulated only at the central intersection point. For this reason, for sensing the displacement caused by the pressure variation and transmitting it only at that point, an external pin is needed. To this purpose, four gold spring loaded contact has been exploited.

Furthermore, due to the sensor's outer circular shape, the stresses applied to it generate an increase in tension that is maximum on the functionalized regions.

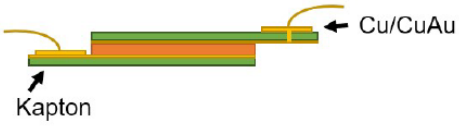

(a) *Structure of the rectangular sensor made with Kapton substrate*

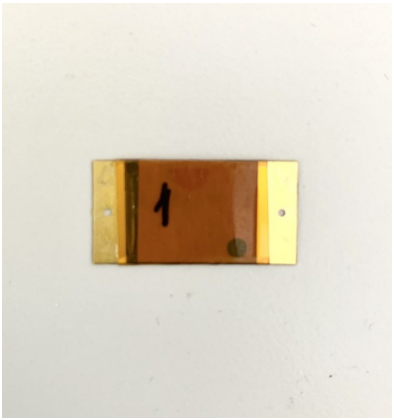

(b) *Final rectangular grapene pressure sensor*

Figure 3.2: Second generation of rectangular graphene pressure sensor.

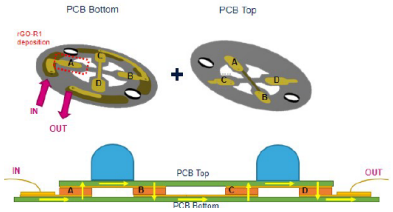

(a) *Structure of the circular sensor.*

(b) *Final rectangular grapene pressure sensor*

Figure 3.3: Second generation of rectangular graphene pressure sensor.

3.2 Sensors characterization

The given graphene pressure sensors developed by The Nanochemistry research group of Strasburg, are extremely experimental and even a datasheet exists. Furthermore, their fabrication process is not at an industrial level, thus each of them may present slightly different electrical properties. Ten brand new rectangular and circular cross sensor has been given from the research group, therefore, with the

purpose of evaluating their behaviour and checking which is the most suitable for cfPWV measurements, both kinds of sensor have been characterized. In particular, they have been subjected to two evaluation procedures:

1. Static resistance evaluation without any weights applied to detect the baseline R values.
2. Constant weight load/unload cycle to understand the sensibility of every single sensor.

For resistance measurements and data collection, is used the combination of the Keysight 34411A multimeter remotely operated by LabVIEW. The data acquired by the multimeter are directly saved in a specified Excel file thanks to a simple LabView program.

3.2.1 Rectangular pressure sensor

First Test

The first test has been performed twice for each of the ten rectangular sensors, with the same methodology but two different setups:

1. SETUP without any weight positioned on the sensitive part of the sensor.
2. SETUP introducing a resin's 3D support on the sensitive part of the sensor to avoid possible deflection. Indeed, since the sensor consists of an extremely thin flexible layer, even a small touch may produce a deflection and thus, may alter the measurement.

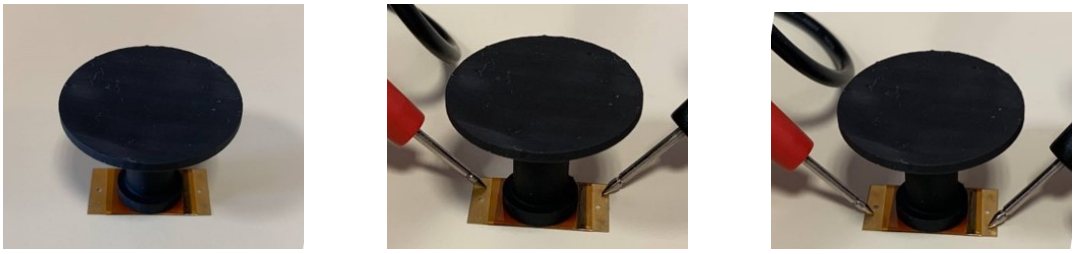

(a) **(b)** **(c)**

Figure 3.4: Illustration of the first test setups. Figure 4.8a shows the first setup while 4.8c and 4.8b shows the second setup.

Concerning the methodology instead, the resistance values were acquired by positioning the digital multimeter probes in two specific points. They were placed

respectively at the top and bottom, with respect to the contact hole. For each of the two positioning, 200 points within the time interval of 45 seconds, were acquired. Finally, they have been processed to obtain a single (average) final resistance value for each sensor.

Experimental results are reported in figure 3.5 where the mean values of the measured resistance are shown along with their standard deviations. Sensor 4 has been removed due to its extremely high, unexpected value. As a result, the graph shows how each sensor is characterized by a baseline resistance of a few hundred Ohms. As evidence, each sensor presents a very different behaviour and this can be justified by the fact that these are devices fabricated in a noncommercial and nonstandardized way. Furthermore, worth of notice the influence of the setup on the resistance values measured. Red coloured columns correspond to the measurement carried out with the 3D support while the blue ones are concerned with the measurements without it. The fact that they differ, as for the case of sensors 2, 4 or 9 is an indication of the extreme sensibility of the device. A minimal deflection has a significant impact on the measured resistance value.

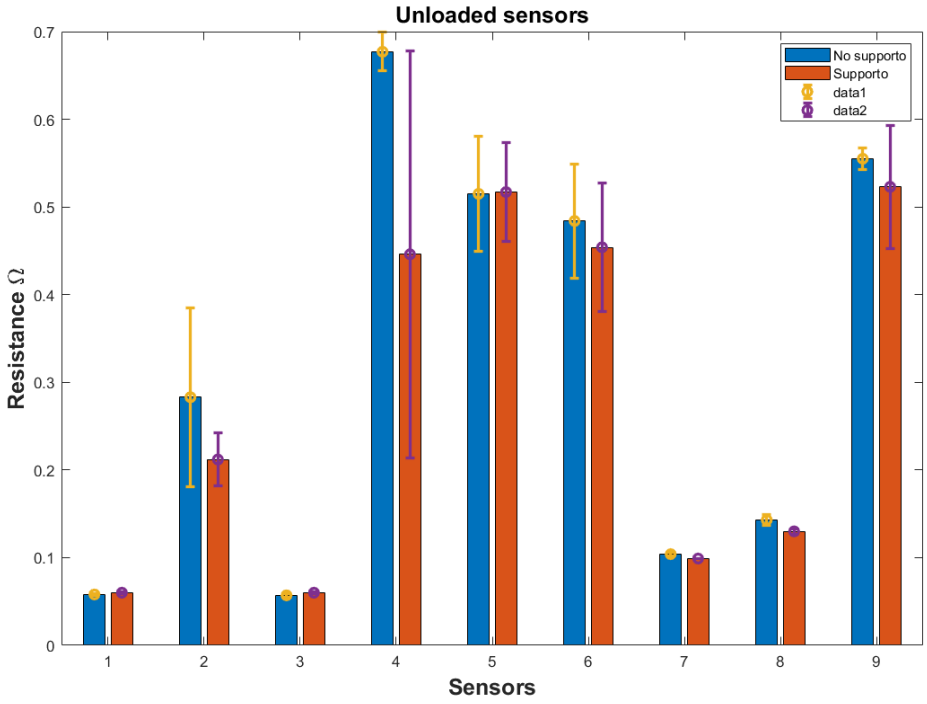

Figure 3.5: Static resistance evaluation of each rectangular-shaped sensor and its correspondent standard deviation.

Second Test

In the second test, it has been investigated the sensibility of each sensor. By implementing a load/unload cycle with gradually increasing loads it has been obtained their correspondent hysteresis cycle. In particular, the weights used had masses of 10 gr, 30 gr, 50 gr, 70, and 100 gr. For each load, a 30 seconds acquisition through the digital multimeter has been executed and then data were post-processed using Matlab.

Being the sensors very sensitive and very small with respect to the set of weights used, a 3D-printed support has been designed. It consists of a circular plate with a diameter size designed according to the circumference of the used masses. During measurement, it has been carefully maintained on the sensitive area allowing for the standardization of the load applied to it. Indeed, the only thing interchanged has been the different weight.

Obtained results have been very different, depending on the sensor under test. For this reason, it has been decided to classify sensors into three different categories: unusable, medium and well "usable" where usable refers to its correct functioning. The categorization criteria were based on the trend of each hysteresis curve and also on the standard deviation corresponding to each load. The following table, 3.1, shows the categorisation of the ten sensors. The steeper the slope, the better the sensor's performance. Furthermore, a comparison of a not usable and a well usable sensor load/unload cycle is shown to provide additional proof on these discrepancies. The difference is remarkable since sensor 1 has a poorly defined trend and high standard deviations in comparison to sensor 10, making it an unsuitable choice for PWV measurements.

Sensor	**Slope**
1	5.5328e-05
8	3.9344e-05
3	2.9508e-05
4	0.0190
2	0.0015
9	0.0016
7	0.0024
6	0.0030
5	0.0038
10	0.0048

Table 3.1: Slope of the characterization curve for rectangular sensors.

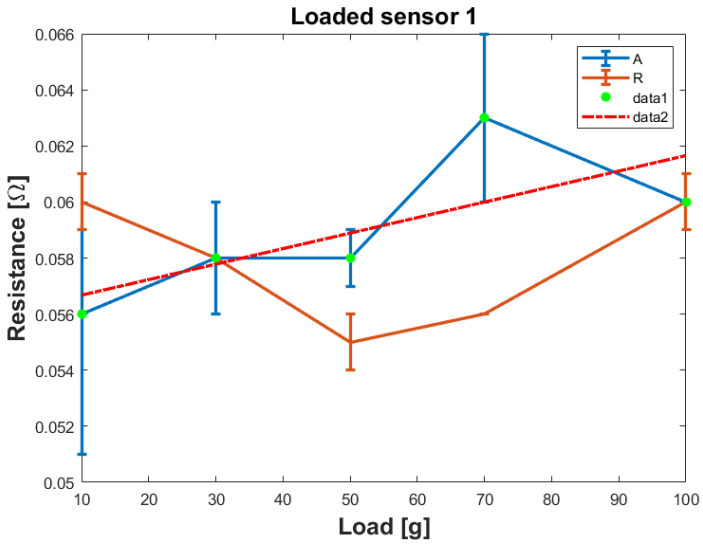

(a) Load/unload cycle of sensor 1

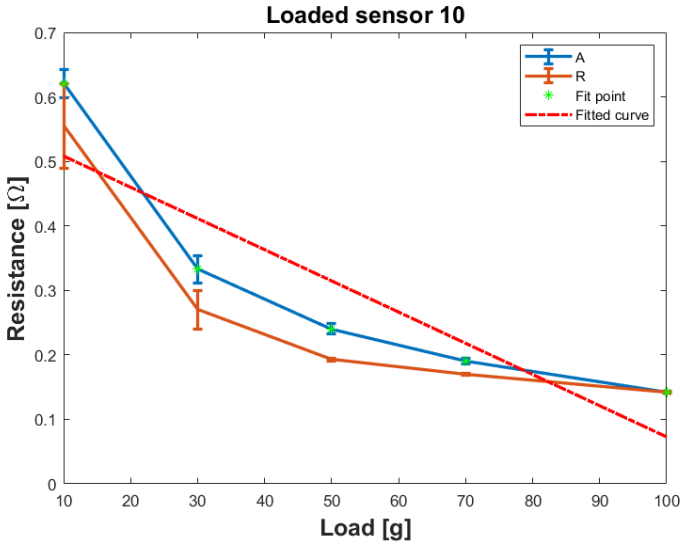

(b) Load/unload cycle of sensor 10

Figure 3.6: Comparison between a not usable and a well usable load/unload cycle of sensor 1 and 10.

3.2.2 Circular pressure sensor

First Test

The test carried out on the circular sensor follows the same methodology as the one developed for the rectangular but had a different setup. Due to the way in which circular sensors are fabricated, it is impossible to position the multimeter probes on the contact area, thus, in order to extract resistance measurements a PCB has been used. The PCB is integrated with the sensor through two bolts and has no component mounted on it but only four spring loaded contact, useful to stimulate the cross at specific points. During characterization, it has been discovered that the two bolts have a not negligible influence on the value measured and thus on the sensor behaviour. For this reason, to carry out the measurement two setups have been used:

1. STEUP the sensor is kept in the wanted position through a 3D support with bolts mounted.
2. STEUP the sensor is kept in the wanted position through a 3D support but has no bolts mounted.

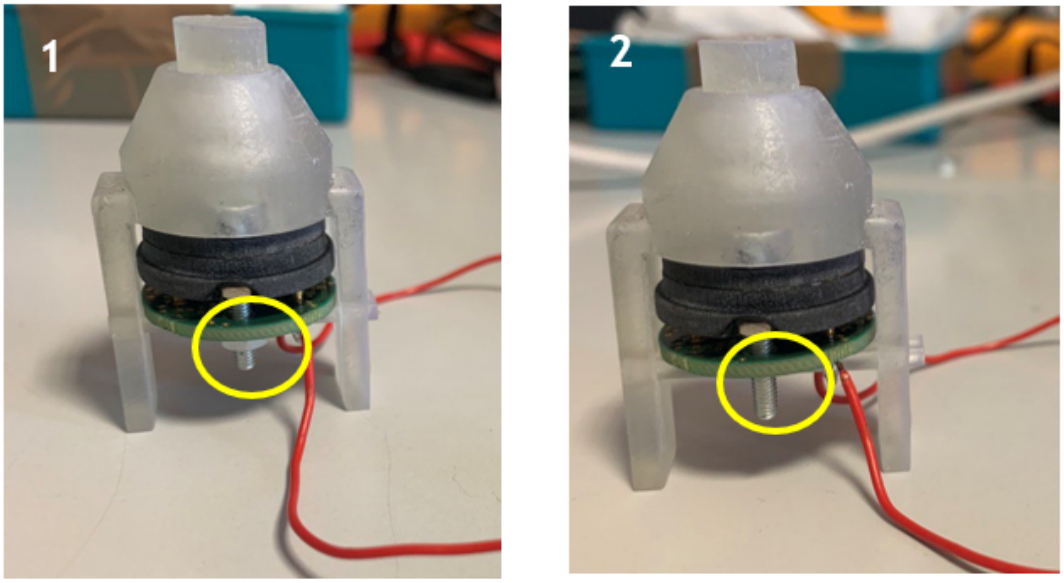

Figure 3.7: Illustration of the two different setup exploited during circular sensors characterization.

Figure 3.8 reports the post-processed dates where even if the standard deviation is small with respect to the rectangular case, the overall trend in terms of the

resistance value is much higher, in the order of few Ω. Neglecting sensor 8, it is remarkable the influence of the bolts that, if present, seems to give much more stability to the sensor.

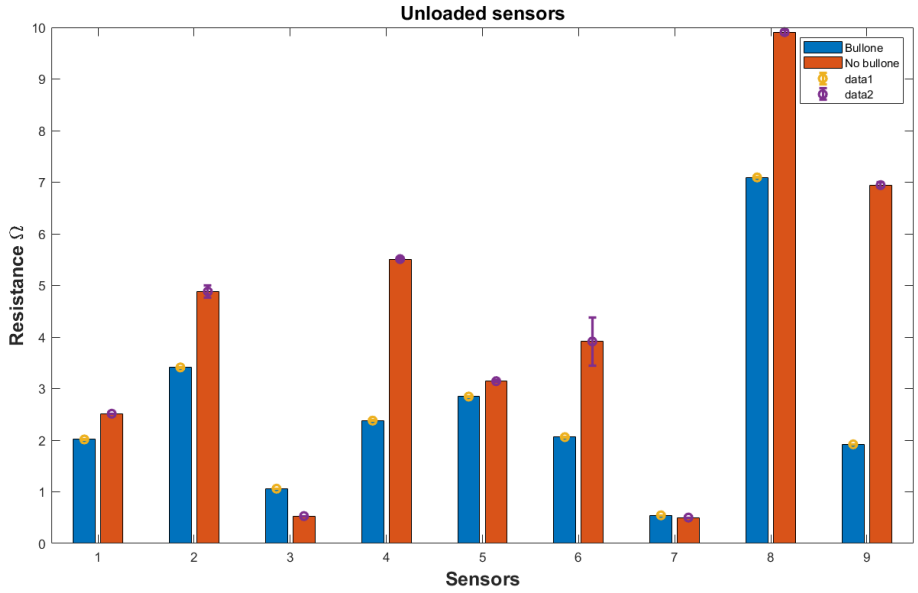

Figure 3.8: Static resistance evaluation of each circular-shaped sensor and its corresponding standard deviation.

Second Test

Based on the first test results, in the second test, it has been decided to use setup 1. The acquisition has been carried out with the same methodology by positioning the weight on the 3D support, as shown in the figure 3.9.

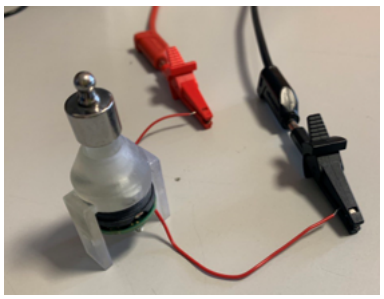

Figure 3.9: Weight loaded sensor during constant weight characterization.

The masses are 10 gr, 30 gr, 50 gr, 70, and 100 gr and for each, a 30 seconds acquisition through the digital multimeter has been executed. The data has been then elaborated in Matlab, where, through the polyfit function the hysteresis curve has been obtained. Due to the very different behaviour, also for the circular sensor it has been decided to do classification. For sake of simplicity, instead of reporting every single curve, table 3.2 summarizes the different slope values of each sensor characteristic curve. The slope of the curve indicates the sensor response to the variation of the applied weight thus, it is an indication of its stability and sensibility. By analyzing these values, circular sensor 5 shows the most suitable behaviour to be integrated into the system while sensor 1 is the worse and thus has not been included. Given the result, a comparison of the not usable and the well usable sensor hysteresis cycle is shown in figure 3.10.

Sensor	Slope
7	7.5000e-05
4	0.0137
3	0.0014
6	0.0016
1	0.0018
9	0.0026
8	0.0028
2	0.0035
5	0.0074

Table 3.2: Slope of the characterization curve for circular sensors.

Understanding the sensors' behaviour has been fundamental to proceeding with system optimization. In particular, through characterization, it has been possible to identify which could be the most suitable for the cf-PWV measurements. In the following chapter, the system architecture will be presented in detail.

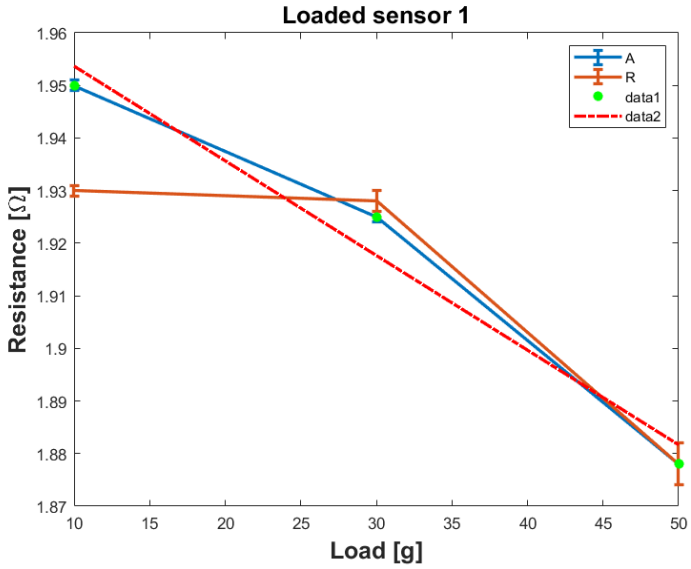

(a) Load/unload cycle of sensor 1

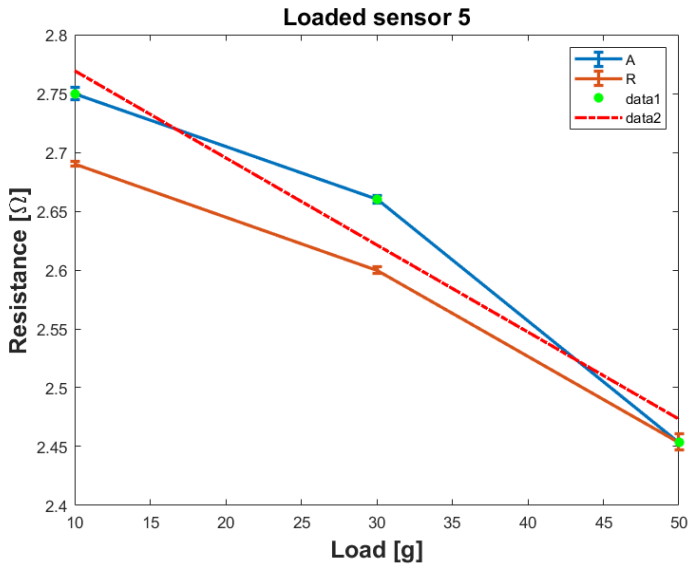

(b) Load/unload cycle of sensor 5

Figure 3.10: Comparison between a not usable and a well usable load/unload cycle of sensor 1 and 10.

Chapter 4

System architecture

The architecture of the already implemented, at early experimental stage, Pulse Wave Velocity estimation system will be discussed in this section. The conditioning circuit is explained first, followed by the system architecture. Lastly, the optimization employed for the signal acquisition and the issues encountered during the cf-PWV assessment are given.

4.1 Signal conditioning circuit

The signal conditioning circuit consists of eight main stages and it has been designed considering two fundamental aspects:

1. The small output resistance of the sensor emerged to be around hundreds of mΩ.
2. The application of interest, which requires a high resolution real-time signal acquisition but at the same time it is highly influenced by several physiological factors.

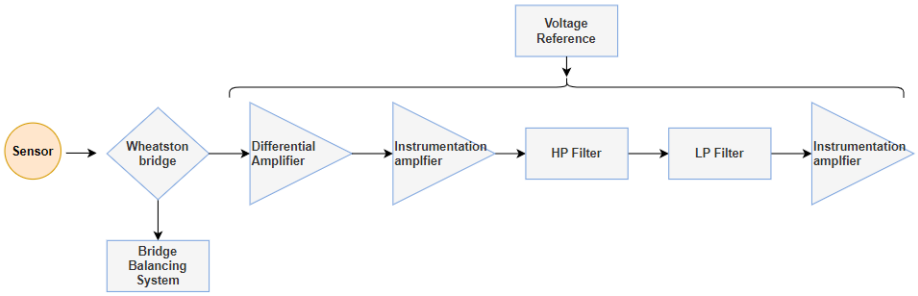

Figure 4.1: Signal conditioning circuit main stages.

Voltage reference A voltage reference is a circuit able to provide a known and fixed potential as long as the system requires it. It is fundamental whenever a real-world quantity is measured because it provides a standard to measure against, the voltage reference. In order to have a portable and low-power consumption device, the system operates with a single power supply delivered directly by connecting it to the laptop. The single power supply is taken from the microcontroller board and it is 3.3 V. The output voltage reference of 1.65 V is then obtained using a linear voltage regulator. To maximize the dynamic, all signals are centred on it. Additionally, the voltage regulator output is fed into a buffer, which decouples the signal source from the rest of the circuit. By preventing it from absorbing too much current from the signal generator, the decoupling boosts its capacity to supply. The components included into the voltage reference ICs are the voltage regulator TLV705165 of Texas Instruments combined at the output with an Operational Amplifier 378. The former is characterized by a low dropout voltage with an accuracy of 0.5%. The latter instated, thanks to low input noise and high gain-bandwidth results to be particularly suitable for portable medical devices.

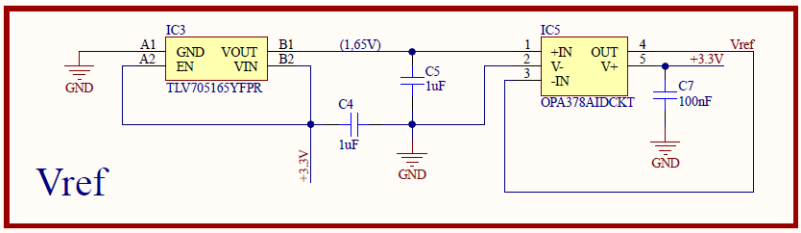

Figure 4.2: Voltage reference circuit.

Wheatstone bridge Since the sensors are characterized by a resistance value of hundred of mΩ the transducer's mechanism is implemented through a current-based Wheatstone bridge configuration. Indeed, given the initial balancing of the bridge, this circuit is ideal for detecting small resistance variations. Furthermore, this configuration has been shown to achieve a resolution of 0.001 Ω [40], which is theoretically adequate for detecting small changes as for the case of the graphene pressure sensor.

Because the system is based on current control, the two currents flowing through the arm must be zeroed in order to establish the equilibrium condition. Referring to figure 4.4, the bridge is initially unbalanced and a current flows from the two nodes A and B (I_{OUT1} and I_{OUT2}). The total output current would be equal to zero if each of the four resistors in the bridge had exactly the same resistance value. Nevertheless, in practice, they never present the same value and are likewise sensitive to time-dependent drifts. Therefore, a transimpedance amplifier is connected to

the bridge and, by varying the offset voltages (V_{off1} and V_{off2}) at its non-inverting terminals, it is possible to impose the voltage levels at A and B nodes necessary for current zeroing. These offset voltages are then subtracted from the output of the Operational Amplifier (OA) in order to not affect the measurements. It results that any variation of the output voltages is exclusively dependent on resistance variations of the sensor.

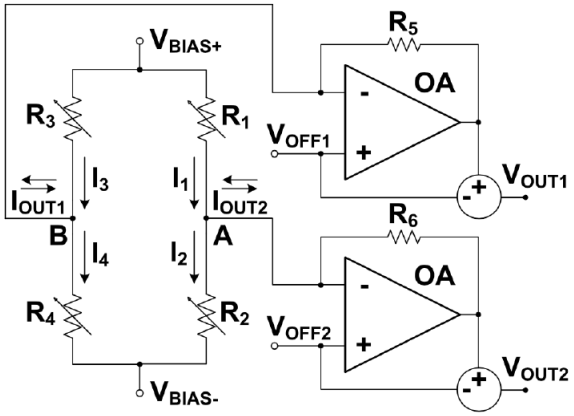

Figure 4.3: Current-based Wheatstone bridge, [41].

Practically, the Wheatstone bridge is implemented in the system with a full-bridge configuration where the four resistances have the same value. Furthermore, in order to have only one branch sensitive to variations, the sensor is in series to one branch. The four resistors are characterized by the same value of 30 Ω, experimentally selected as the smallest value that can handle the high current that flows in the bridge. The purpose of this choice is to maximize the system's sensitivity which can be calculated as the variation of the output due to a variation of the inputs, in this case current. Knowing that the current flowing through the bridge can be obtained as:

$$\begin{aligned} I_{OUT} &= I_{OUT2} - I_{OUT1} = \\ &= \frac{V_{BIAS}}{2} \frac{R_2 R_3 (R_5 - R_4) - R_4 R_5 (R_3 - R_2)}{R_4 R_5 R_2 R_3} = \\ &= V_{BIAS} \frac{2\Delta R_0}{(R_0 + \Delta R_0)(R_0 - \Delta R_0)} \end{aligned} \tag{4.1}$$

The sensitivity of the system will result in:

$$S = \frac{\delta I_{OUT}}{\delta \Delta(R_0)} = V_{BIAS} \left(\frac{1}{(R_0 - \Delta R_0)^2} + \frac{1}{(R_0 + \Delta R_0)^2} \right) \cong 2 \frac{V_{BIAS}}{R_0^2} \tag{4.2}$$

According to 4.2, the system becomes less sensitive whenever the resistance R_0 is too high.

Bridge balancing system In order to appreciate only the dynamic variation of the sensor resistance, a bridge balancing system is used, consisting of two main parts:

- **Current reading**: responsible for reading the current that flows in the bridge branches. It reads and amplifies the voltages falling on the two resistors, R1 and R7, using an Instrumentation Amplifier INA333. This component offers a low offset voltage, great common-mode rejection, and high precision over the industrial temperature range, making it particularly suited as a bridge amplifier. Considering that its feedback resistance is set to 100kΩ, the output voltage will be amplified with a factor of 2. Indeed, according to its datasheet, the gain can be calculated as:

$$G = 1 + \frac{100k\Omega}{R_g} \tag{4.3}$$

  The two outputs of the INAs, are then connected to two different ADC channels of the Pyboard D-Series SF2W. In this way, on the basis of the voltage drop sampled, the current is calculated via firmware.

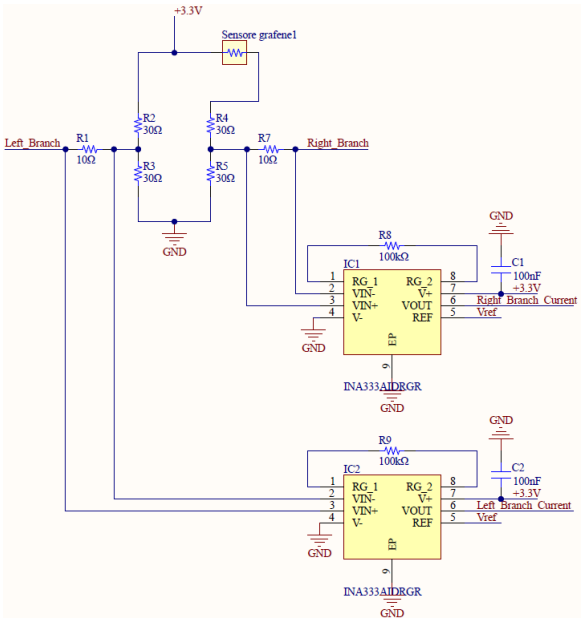

Figure 4.4: Current reading circuit.

- **Current nulling**: responsible for zeroing the current, this circuit section is based on a Digital-to-Analog Converter DAC102S085. This component, able to ensure a rail-to-rail voltage output and working at clock rates up to 40MHz [48], set the offset voltage V_{off1} and V_{off2} at the input of the transimpedance amplifier stage. This latter is the other fundamental component of this section, necessary in order to convert the bridge's outgoing current I_{out1} and I_{out2}, into voltages. Its feedback resistance is set to 7.5 Ω thus the output voltage will result from:

$$V = -(7.5\Omega)I \tag{4.4}$$

  Finally, in order to obtain a single unique reference voltage, set to 1.65V, the offset voltages are subtracted from the output of the transimpedence amplifier thanks to a differential amplifier. Considering that its four resistors are set to the same value of 1.2 kΩ, the output can be obtained as:

$$V_{OUT} = -V_1\frac{R_2}{R_1} + V_2\frac{R_4}{R_3} \tag{4.5}$$

  To physically implement this two op-amp based stages a single component has been used, the OPA4347. This component is the quad-version of the OPA347 which is able to provide a rail-to-rail input and output plus a low power consumption (34µA per channel maximum), making it ideal for portable applications. As reported in the figure, op-Amp A and B exploits the transimpedence stage while C and D the differential one.

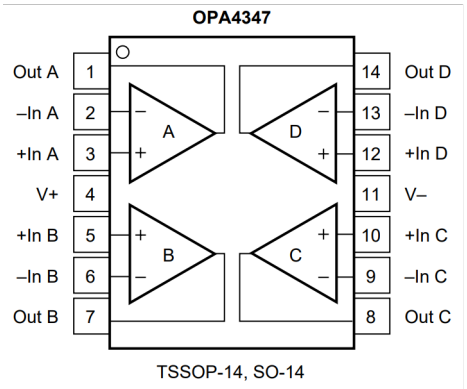

Figure 4.5: MicroPower Rail-to-Rail Operational Amplifier 4347 pin out description, [46].

First amplification stage The output signal of the sensor converted by the transimpedence stage is in the range of tens of mV, for this reason, the system

presents a first stage of amplification. It is implemented using an Instrumentation Amplifier INA333, that allows to set any gain from 1 to 1000 by selecting a precise value of its external resistor R_g. In this application, the selected value is $R_g = 1.1k\Omega$ leading to a gain $G = 92$.

Filtering stage During the acquisition of the signal, electrical noise and any possible network interference must be eliminated. To this purpose, the system presents two filtering stages: a high pass filter, characterized by a cut-off frequency of $F_c = 0.1Hz$ in order to remove the electrical noise, and a low pass filter, characterized by a cut-off frequency of $F_c = 20Hz$ to remove the network interference. Both HP and LP filtering is obtained by exploiting a third-order Sallen Key filter which provides adequate performance in terms of delay and attenuation. The component used to implement the filter in the circuit is the OPA4347.

Second amplification stage This last stage of the system is a Programmable Gain Amplifier, responsible for better adapting the amplitude of the acquired signal to the dynamic of the ADC. Indeed, it has to be considered that the arterial pulse can widely change in amplitude due to different physiological factors; depth of the arteries, the thickness of the subcutaneous fat, and so on. The PGA is implemented through a INA333, which allows for the use of a single trimmer to modify the gain. To make the gain programmable a series of switches, controlled by the CMOS analogue multiplexer MAX4781, is used. By changing the logic value of the input pin of this latter, the switches connect the Instrumentation Amplifier to the specific resistance. The table 4.1 reports the eight values of gain and its corresponding resistance, which is possible to set.

Resistance (Ω)	**Gain**
2040	50
1000	101
560	180
400	251
300	334
220	455
130	770
100	1000

Table 4.1: Resistance and respective gain values used in the programmable amplifier.

4.2 Initial configuration based on Pyboard D-series

The architecture of the pulse wave velocity estimation system is reported in figure 4.6, where a fundamental component of the entire system is shown, the Pyboard D-series SF2W. Infact, this microcontroller module running Micropython, is responsible for the power supply of the conditioning circuit and the management of the signal acquisition. The Pyboard and the needed specific peripherals employed are integrated with a main PCB, in which part of the conditioning circuit already illustrated in the previous section, is implemented. These two elements form a unique main unit that, on one side is responsible for the USB data transmission to a laptop and on the other, is connected to two other identical PBCs implementing the other section of the conditioning circuit.

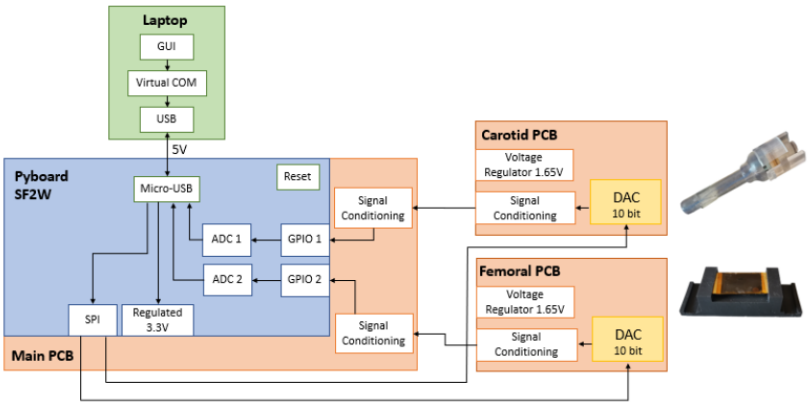

Figure 4.6: Architectural diagram of the system configuration based on Pyboard D-series SF2W.

Pyboard D-series SF2W The microcontroller embedded into the board, produced by STMicroelectronics, is the STM32F723IEK. Is based on the Arm® Cortex®-M7 32-bit RISC core, that can operate up to 216MHz frequency with a single floating point unit precision. It has up to 512 Kbytes of Flash memory, 528 bytes of OTP memory and the possibility to use external memory thanks to the 32-bit data bus, [42].

The main peripheral used for the purpose of the application has been:

- **Voltage Regulator**: the LD39130S, a 3.3V LDO voltage regulator integrated in the Pyboard D-series SF2W that allows for external components powering. It has a low dropout voltage at the maximum load (typically 300mV) and

can deliver output current up to 300 mA. It's suitable for wearable low power applications due to the low quiescent current and low noise characteristics.

- **Analogue to digital converter**: The STM32F723IEK has 3x12 bit analogue to digital converters (ADC), with up to 24 channels, available on 16 pins [42]. Is used to sample and convert the voltage from the two bridge branches of each channel (carotid and femoral) and the filtered and amplified signals at the last stage of the conditioning circuit.

- **Serial Peripheral Interface**: The STM32F723IEK is provided by 5 SPIs communication interfaces, two of them has been exploited for managing the communication with the DAC. Specifically each of these peripheral is responsible for sending the voltage value to be converted via software to DAC.

4.2.1 Support Design

The PWV estimation system based on Pyboard D-Series, implements two resin supports for holding the sensors. They are specifically engineered in order to facilitate the use of the device during the carotid and femoral assessment, carried out by the clinician. Since the sensors have been fabricated in two different shapes, it has been necessary to design two different, customized, supports for each.

Optimized rectangular support

The rectangular sensors consist of a thin layer with golden electric contacts on both sides, therefore the starting configuration consists of a support that has the same shape as the sensor and provides a slot for the insertion of it. This design has been conceived to be operator independent thus, it also implements two side flaps for being attached to an elastic band. The important point considered for the design of the sensor support were:

1. A minimal thickness of the upper part, to favour the adhesion of the sensor to the patient's skin.

2. An increased thickness of the bottom part, to increase the pressure applied to the patient skin and obtain a better pulse wave signal detection.

Subsequent device optimization led to changes in the configuration of the system. The rectangular sensor has been directly integrated with the rectangular PCB thanks to two spacers on which it has been welded. Having the sensitive element close to the conditioning circuit allows for reducing the electrical noise and avoiding connection wires. For this reason, a new holder has been designed, taking into account the same criteria already indicated, which are required to support effective

signal detection. It is designed so as to fix the "rectangular PCB-sensor" block on its inside but at the same time presents a thickness of only $5mm$ to prevent the system from becoming excessively stiff. To achieve this interlocking configuration, pillars with various thicknesses and heights needed to be designed. They were intended to be placed at particular locations on the printed circuit board (PCB) to ensure mechanical support without affecting any of the components soldered onto it. Furthermore, it includes two side flaps useful for device placement during the acquisition phase.

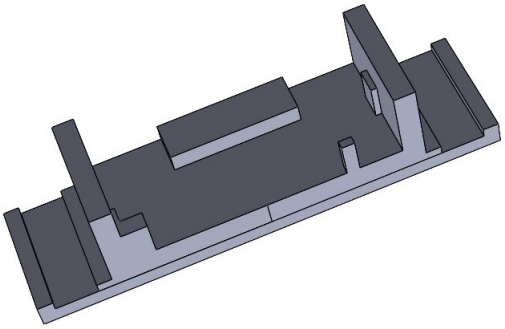

Figure 4.7: 3D rectangular designed support for the sensor.

Optimized circular support

As deeply detailed in paragraph 3.1, the circular sensor is made up of two flexible PCBs with distinct tracks of gold electrical contacts that allow it to perceive the pressure applied in the central point and transduce it with high sensitivity. These two flexible PCBs are held together with a customized case that prevents the two sheets to slip into each other. This latter consists of two 3D printed circumferences, clamped by two screws. Furthermore, being empty in the middle, a movable element can be inserted to stress the sensor, while the screws act as fixing points to interlock the sub-units. Based on this, the configuration for the circular cross-sensor consist of a support case integrated in a pen-shaped holder. The support case is a cap, with a truncated cone shape conceived to reduce as much as possible the contact area when positioned on the acquisition site. Within the cap, it is inserted a tip, responsible of transmitting the detected displacement from the skin to the sensor. To this purpose, its lower part is semi-spherich in order to apply the stimuli only at the centre point of the cross sensor. Its upper surface instead is flat and circular so as to increase the contact surface. Subsequent device optimization led to changes in the system configuration. In particular, a new Printed Circuit Board, with a specific circular shape, has been designed to be integrated directly with the sensor. Nevertheless, the circular PCB should be supplied by the Main PCB through wires,

for this reason, a holder optimization has been necessary. The two important constrains considered during the re-design were:

1. Creating a not fixed configuration for the holder, to guarantee the possibility of access the electronics.

2. Ensure a fixed position of the electronics once encapsulated inside the support.

Starting from these constraints, the first thing has been the design of a support consisting of two separate sides, joined together thanks to their complementary configuration. This, allowed for interlocking them and obtaining a unique pen-shaped holder. Then, to ensure a fixed position of the device structure once encapsulated inside the holder, two thick rectangular pillars are present. Finally, to provide the suited space for the insertion of the sensor with the cap, the upper part of the pen has been designed with two side-bands characterized by a curved profile. The tip has been maintained in its original shape.

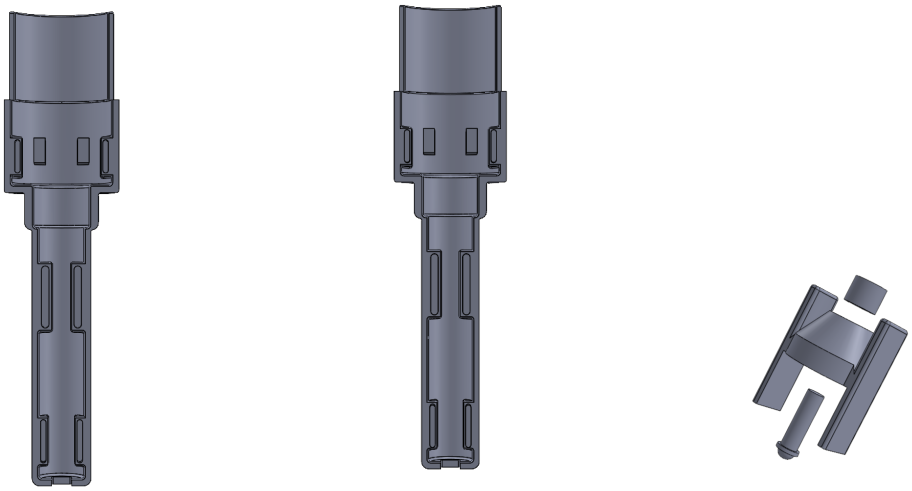

(a) Left side of the pen. **(b)** Right side of the pen. **(c)** Tip of the pen.

Figure 4.8: 3D pen-shaped configuration designed for the circular sensor.

Both the rectangular and the circular support have been designed using SolidWorks as a CAD tool and subsequently have been printed using the 3D resin printer Form3, from Formlabs.

4.3 Signal acquisition limits

The signal acquisition is managed by the combination of a specific firmware, controlling the Pyboard, and a Graphical User Interface, for the real-time display of the data.

The acquisitions have been carried out to test the new system configuration based on the new generation, previously characterized sensors, combined with the newly designed holders, on a human subject. Specifically, the chosen system setup includes the circular cross sensor utilized to evaluate both the femoral and carotid sites. In collaboration with the "A.O.U. Città della Salute e della Scienza di Torino" the device has been tested on a volunteer. The measurement, carried out by the clinician, has been obtained by positioning the two pen shaped probe on the carotid and femoral sites.

The first step necessary for the signal acquisition was managed by software; through the Graphical User Interface, it must be performed firstly the bridge balancing then, once obtained, it is possible to start the acquisition that allows for realtime visualization of the signals on the laptop display. During tests, the system has reported unexpected behaviour. Figure 4.9 and 4.11, report the acquired data, that have been plotted on Matlab in order to better analyze the trend. As they illustrate, both carotid and femoral channel are capable of acquiring at least one first pulse wave. However, they tend to saturate and are, very likely, unable to guarantee acquisition stability. This is not acceptable for the purpose of the application, where the clinics should be able to evaluate the vital parameter in realtime without losing any information.

A step back has been necessary and an in deep analysis has been performed. A first analysis regarded the mechanical stability of the configuration. The circular sensor is integrated with the circular PCB through two screws and fixed with two blots. It has been discovered that depending on how much the bolts are tightened, the sensor response changes. This point made it clear the PCB-Sensor unit cannot be interchangeable using other sensors because it shows to be dependent upon how firmly the screws are tightened. Nevertheless, focusing on the single configuration, after determining the degree of freedom necessary to provide a reliable sensor response, circular spacers were developed and printed using the 3D Form resin printer. They were simple cylinders designed with a diameter higher than that of the screws. They have an empty core useful for the insertion of the screw body. Considering fixed the mechanical part, another session of test has been done and the same poor results in terms of signal acquisition have been obtained. For this reason, another important investigation concerns the electronics. To understand if the lack of stability could be related to some of the electrical components of the conditioning circuit, the circular PCB alone has been tested.

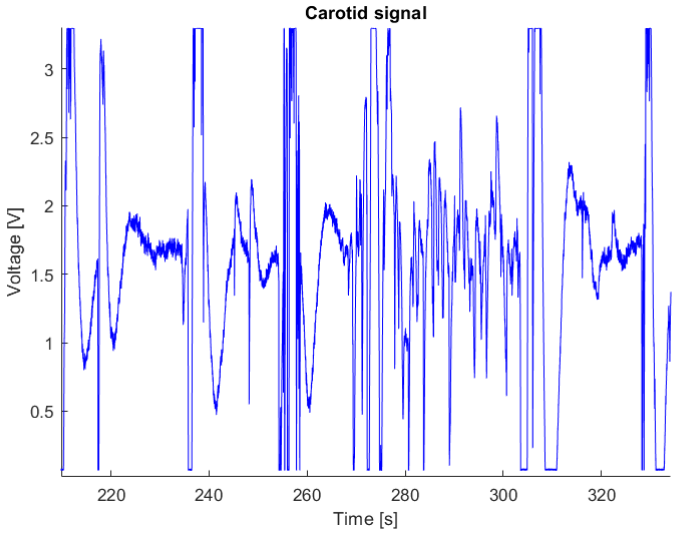

Figure 4.9: Pulse Wave Signal acquired at the carotid site plotted on Matlab to investigate the behaviour of the sensor.

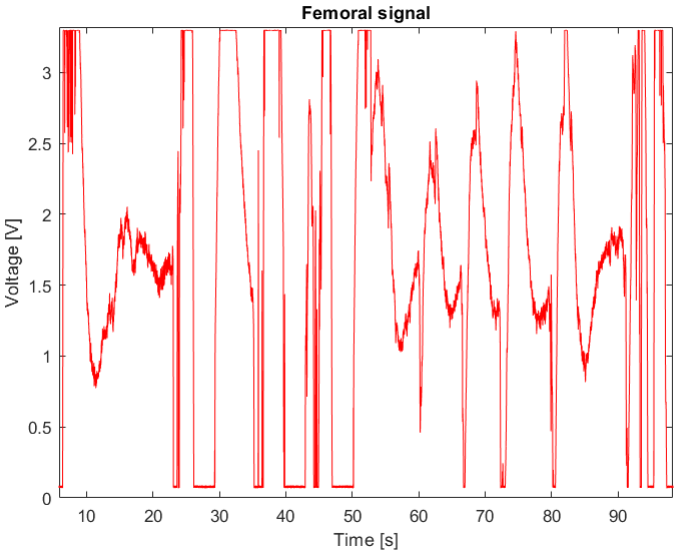

Figure 4.10: Pulse Wave Signal acquired at the femoral site plotted on Matlab to investigate the behaviour of the sensor.

With the help of a Programmable DC power supply, the RIGOL DP832A, the PCB has been supplied with 3.3 V and 0.1 A current, in order to check for its current consumption. The results have revealed a consumption of 73 mA. Considering that this value refers to the PCB only, is quite huge. However, the reason for this was found on the four 30Ω Wheatstone bridge resistances since these components show to become very hot after a few minutes they are powered. They are 0805 inch resistors with a power rating of 0.5W, however, as matter of fact the power across the resistor is not kept under its maximum ratings.

These important outcomes led to a step back. Despite the system demonstrating its capability in acquiring signals, electrical stabilization seemed to be necessary. To this purpose, the microcontroller board has been changed from the Pyboard D-series SWF2 to an STM32F4 series Discovery Kit. In the next section, the new system configuration will be presented in detail.

4.4 Final configuration based on STM32Discovery Board

Concentrating on the electrical stability of the device, the read out system has been modified. The same signal conditioning circuit has been maintained but adapted to a new microcontroller board, the STM32Discvoery Kit.

4.4.1 Signal conditioning circuit optimization

Starting from the conditioning circuit the first change involved the voltage reference section which, due to the electrical issues encountered during tests has been modified. First of all the TPS79533DCQ voltage regulator has been integrated into the circuit. This component is a linear step-down voltage regulator that takes as input the 5V provided by the Discovery board and reduces them to a lower, fixed output voltage of 3.3V. The main reason for this change refers to the power consumption limits of the 5V pins. Indeed, according to the Discovery Reference Manual, whenever this pin is used as an output power supplier its maximum power consumption must be lower than 100 mA. This turned out to be an important limitation. By doing a simple analysis based on the issues reported in section 4.3, if a single sensors-PCB block consumes 80mA, considering that this quantity must be doubled (being two the acquisition channels) the overall current consumption results to be higher than 100 mA and the pin results to be unusable.

The second change implemented is the integration of the NCV8114LDO voltage regulator whose main function is to centre all signals on the same reference voltage equal to 1.65V. This component is suitable since it has a very low quiescent current of 50 µA, low dropout voltage and a ±1% accuracy at Room Temperature [45].

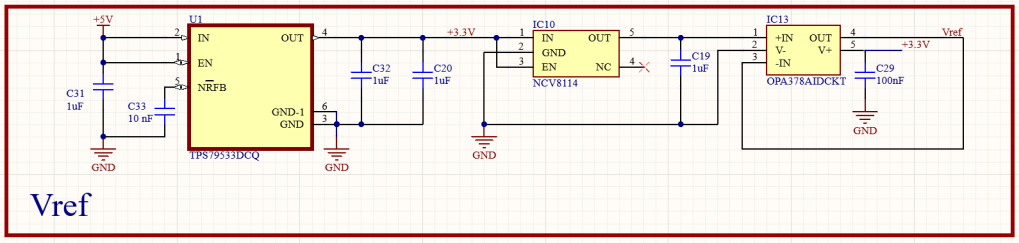

Figure 4.11: New voltage reference circuit configuration.

4.4.2 Discovery Kit STM32F429I

Besides the conditioning circuit, the major changes regarded the microcontroller board that has been changed with the Discovery DISC1-STM32F429I, based on the STM32F429 MCU. This Discovery Kit, is an integrated development board which allows for modular design and customization thanks to the several features offered by the STM32 MCUs and MPUs. It is a low-cost but high performance solution based on the STM32F429 32-bit ARM® Cortex™-M4 RISC core, operating at a frequency of up to 180 MHz [52]. The powering of the board can be obtained either using a 5V DC external source or through the USB ST-LINK, connecting the board to the host PC via USB. Furthermore, the DISC1-STM32F429I Discovery board is capable of providing a 3V or 5V supply voltage. The 5V power supply is the one used in this project for powering the entire conditioning circuit. The adopted Discovery Kit includes also a 2.4" LCD-TFT display controllers and communication peripherals such as I2C and SPI.

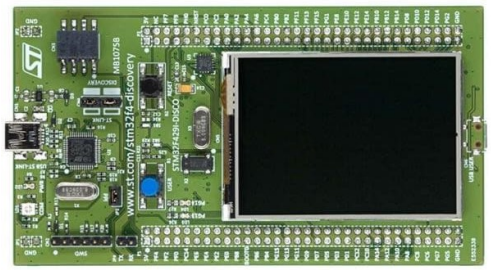

Figure 4.12: Illustration of STM32F429I-DISC1 board.

The peripherals used for the application have been: USB for the data transmission, ADC input pins for the signal sampling, SPI for interfacing with an external DAC (part of the conditioning circuit) and six GPIOs pins for the implementation of

a Programmable Gain Amplifier. Hereafter, all these used peripherals will be described in detail:

- **Microcontroller unit (MCU)** The microcontroller produced by STMicroelectronics and embedded into the Discovery Kit, is the STM32F429ZI [51]. It is based on the Arm® Cortex®-M4 32-bit RISC core, that features a single Floating point unit (FPU). The MCU includes high-speed embedded memories as flash memory up to 2 Mbyte and SRAM up to 256 Kbytes. The microcontroller offers up to 17 timers running up to 180 MHz. It also includes up to 168 I/O ports with interrupt capability and up to 6 SPIs (45 Mbits/s).
- **Analog-to-digital converter (ADC)** The microcontroller is featured by three 12-bit successive approximation analog-to-digital converters. Each of them includes up to 19 multiplexed channels for measuring signals from 16 external sources. In this application six of them have been initialized, four (two for the Caroitd and two for the Femoral site) are involved in the balancing algorithm while the remaining two are used to sense and convert the filtered and amplified signal at the last stage of the conditioning circuit. The A/D conversion of the channels can be performed in single, continuous, scan or discontinuous modes. For this application, the channels are configured in single conversion mode.
- **Serial peripheral interface (SPI)**

  The STM32F429I-DISC1 board is provided with up to six Serial Peripheral Interface, operating either in Full-duplex synchronous transfers or Simplex (half-duplex) synchronous transfers. The data frame is 8 or 16 bit large and can be transferred with bauderate up to 45 Mbits/s. The SPI is a high-speed synchronous serial protocol based on a single master to multiple slave architecture. The communication mode is set by the master and in the case of full-duplex mode, the hardware communication lines involved are four:

  - Serial Clock (SCLK), it is the output clock set by the master, needed to synchronize the data to the rising or falling edge.
  - Chip Select ($\overline{CS}$), it is the hardware slave selector used by the master to indicate the slave to communicate with.
  - Master Out Slave In (MOSI), it is the master data output line.
  - Master In Slave Out (MISO), it is the slave data output line.

  There is also the possibility to use the SPI in half-duplex mode. In this case, the architecture configuration changes and uses three wires only: Serial Clock (SCLK), Chip Select ($\overline{CS}$) and a single data communication line. The line, known as DI/O, connects the MOSI of the master with the MISO of the slave.

In this application, the SPI peripherals configured are SPI3 and SPI6, one for each PWV assessment site. They interface with the DAC102S085, setting at its input the offset voltage to be converted and directed at the transimpedance amplifier.

The DAC102S085 component is a DUAL 10-bit voltage-output digital-to-analog. It has a 16-bit input shift register that controls the outputs to be updated, the mode of operation, the power-down condition, and the binary input data. Both outputs can be updated simultaneously or individually depending on the setting of the two modes of operation bits,[48].

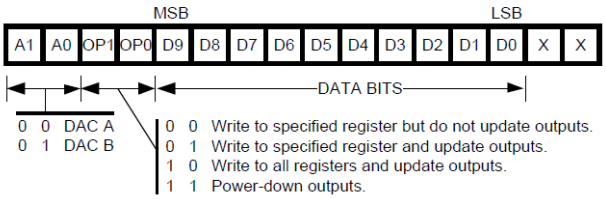

Figure 4.13: Input Shift Register of DAC102S085, [48].

To establish communication with it, it has been necessary to consider its serial timing diagram. As reported in the figure the write sequence starts setting the SYNC line low. Then the data on the DIN line is clocked into the 16-bit serial input register on the falling edges of SCLK. Furthermore, SYNC must not be brought low concurrently with a falling edge of SCLK in order to prevent data into the shift register from being misclocked. On the 16th falling clock edge, the last data bit is sampled and the DAC output is updated.

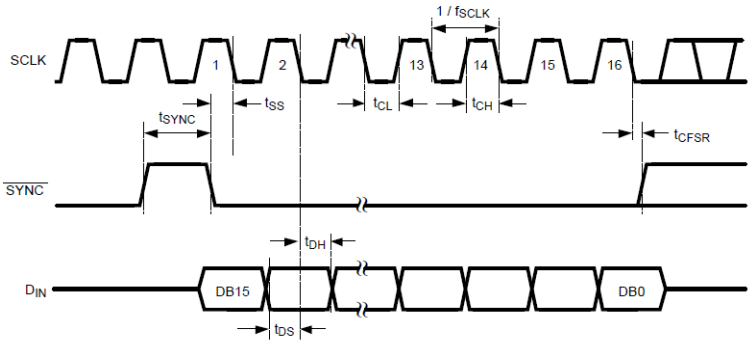

Figure 4.14: Serial Timing Diagram of DAC102S085, [48].

Starting from figure, the Polarity and the Phase of the SPIs have been set respectively to CPHA=1 and CPOL=0.

- **General-purpose input/output (GPIO)**

  To implement the gain selection for the Programmable Gain Amplifier already presented in detail in section 4.1, six General-purpose input/output pins have been initialized, 4.2. Then, they have been configured to be low or high depending on the desired amplification gain.

GPIO	Channel
PB4	CAR
PB7	CAR
PC8	CAR
PE2	FEM
PE3	FEM
PE4	FEM

Table 4.2: Discovery board GPIOs configured for the implementation of the PGA.

4.4.3 Printed Circuit Board design

The Pulse Wave Velocity estimation system is implemented with a configuration that splits the signal conditioning circuit into two section implemented in two separate PCBs:

- **Peripheral PCB**: consisting of the Wheatstone bridge, the current reading system and the first stage of amplification, it is directly integrated with the sensor. Since the conditioning circuit is the same for both carotid and femoral channels, two identical PCBs are integrated into the system. Furthermore, taking into account the shape of the sensors two different PCB versions exist the rectangular and the circular. Both are directly integrated with the sensors as shown in 4.17.

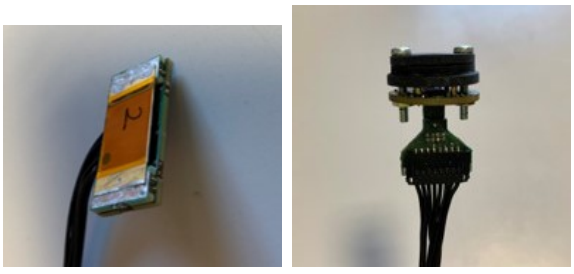

(a) Rectangular configuration **(b)** Circular configuration

Figure 4.15: Rectangular(a) and Circular(b) sensor-pcb configurations.

- **Main PCB**: consisting of the filtering stage and the second amplification stage, it should be integrated with the micro controller board. Starting from that, considering minimizing the wire connections and the possible electrical noise, it has been conceived with a shield configuration, 4.17. Through the P1 and P2 header connectors lines, it is possible to directly integrate the Main PCB with the bottom of the Discovery broad obtaining a compact configuration.

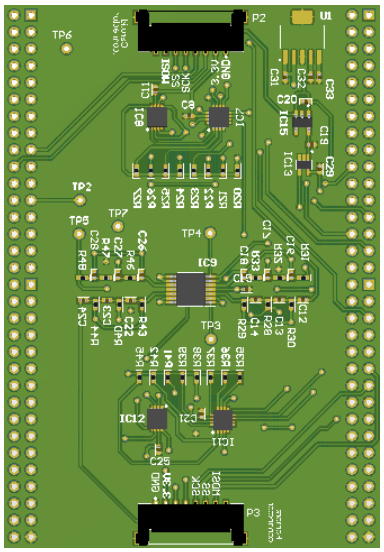

Figure 4.16: PCB layout of the bottom layer.

The PCB bottom layer, where all the components have been placed, is shown in figure 4.16. Since the Main PCB should manage both channels at the same time its layout result symmetric to the PCB centre. The interaction with the Discovery board is obtained through 9 headers (for each channel): 2 are used for the power supply (5V and GND), 3 for the ADC input channels, 3 for the SPI connection (SCLK, DIN, CS) and finally 3 for the Programmable Gain Amplifier.

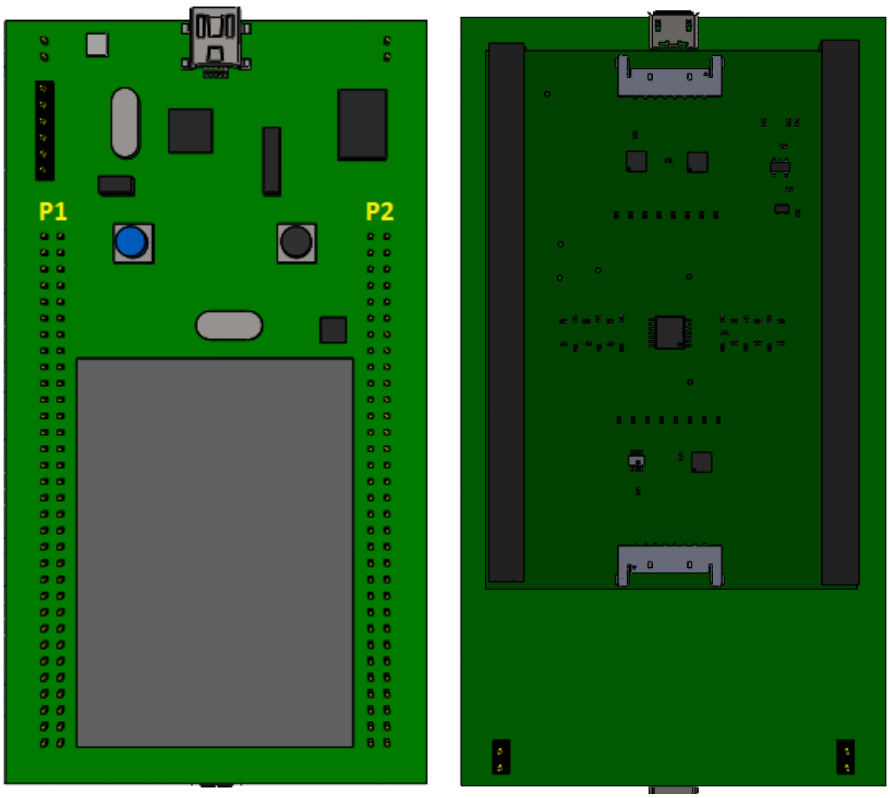

(a) Top view **(b)** Bottom view

Figure 4.17: CAD illustration of the shield configuration obtained integrating the PCB on the Discovery board through specific female header connectors.

Chapter 5

Software Implementation

In this chapter will be presented the software implementation carried out to implement the new system configuration. First, the developed firmware for the STM32Discovery Board will be described in detail, followed by an explanation of the essential changes that have been made to adapt the Graphical User Interface and allows for real-time signal acquisition.

5.1 Firmware development

Given the necessary hardware changes, a new firmware running on the STM32F429I-DISC1 board has been developed. The program is written in C language in the Keil Vision®environment. Understanding the process flow has been the starting point for its correct implementation since the firmware developed for this application should handle multiple aspects at the same time. The designed flow chart is depicted in figure 5.3.

Once the device is connected via USB through the host PC to obtain the 3.3V power supply, the firmware proceeds with the peripherals initialization. A small section of the code is reported in listing 6.1 where, after the system clock and the ILI9341 TFT-LCD initialization, the key functions executed are:

- `USBD\_Init(\&USBD\_Device, \&VCP\_Desc, 0);` functions and the cor‡ related supported classes, for the initialization of the USB, configured as a device with a Full-Speed data transfer.
- `ADC\_config();` function, responsible for the initialization of the three ADC peripheral. It configures ADC1, ADC2 and ADC3 in single conversion mode triggered by an external timer, Timer 3.

- `TIM3\_Config();` function, responsible for the initialization of the timer 3 peripheral whose sampling frequency is set to 1 KHz configuring the timer Period = 9, the Prescaler = ((SystemCoreClock/2)/10000) - 1 and the Counter direction = Up.
- `DAC1\_SPI\_Init()` and `DAC2\_SPI\_Init()` functions, responsible for the initialization of the SPI6 and SPI3 peripherals, respectively. Since they are exploited to communicate with the external DAC102S085, the SPI mode is set to MASTER with a 2LINES direction and LOW polarity, in accordance to the DAC serial timing.
- `GPIO\_Init();` function, responsible for the initialization of the six GPIOs already detailed in section 4, table 4.2. They are configured in Output Push Pull Mode.
- `EXTILine0\_Config();` function, responsible for the EXTI controller initialization. The EXTI input line configured is the zero line with an interrupt priority set to 5.

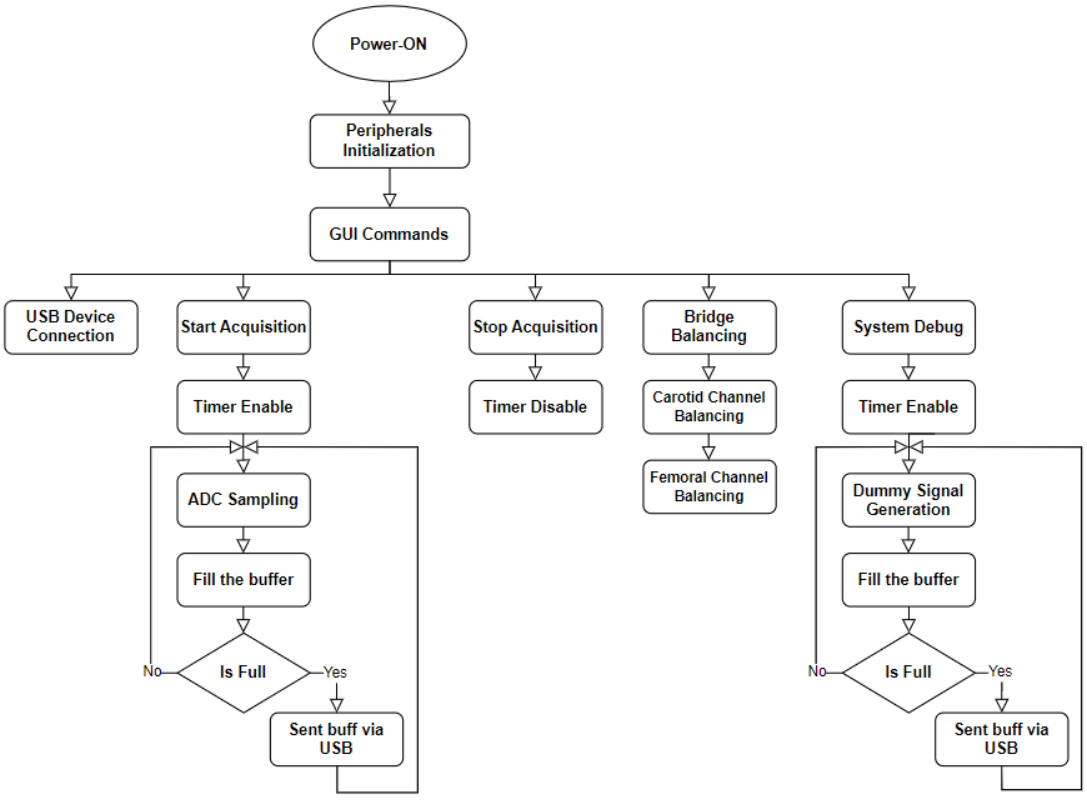

Figure 5.1: Firmware flow chart illustration.

Listing 5.1: Pheriperals initialization.

```
int main(void)
{
    HAL_Init();

  /* Configure the system clock to 168 MHz */
  SystemClock_Config();

  /* Init Device Library */
  USBD_Init(&USBD_Device, &VCP_Desc, 0);

  /* Add Supported Class */
  USBD_RegisterClass(&USBD_Device, USBD_CDC_CLASS);

  /* Add CDC Interface Class */
  USBD_CDC_RegisterInterface(&USBD_Device, &USBD_CDC_fops);

  /* Start Device Process */
  USBD_Start(&USBD_Device);

  /* Init ILI9341 with LTDC on STM32F429 Discovery board */
  ILI9341_SPI_Init();
  TM_ILI9341_Init();
  TM_ILI9341_Rotate(TM_ILI9341_Orientation_Landscape_2);

  /* Fill layer 1 */
  TM_ILI9341_Fill(ILI9341_COLOR_BLUE);

  /* Put some text */
  TM_ILI9341_Puts(5, 10, "    WaVESystem - Graphene     ",&
    TM_Font_11x18, ILI9341_COLOR_BLACK, ILI9341_COLOR_WHITE);

  ADC_Config();
  TIM3_Config();
  DAC1_SPI_Init();
  DAC2_SPI_Init();
  GPIO_Init();
  EXTILine0_Config();

  /* Run Application (Interrupt mode) */
  while (1)
  {
    if (CMD_state == CMD_AVAIL)
    {
        CMD_state = CMD_NOT_AVAIL;
        command_decode();
    }
  }
}
```

After the necessary initialization, the firmware waits for the command from the Graphical User Interface that, once received, is managed through the `command_decode();` function. Section x reports the function implementation, where the incoming string is decoded to allow the execution of the correspondent task. Following the firmware flowchart, the possible operation cases are four, however, an execution order exists.
The first step should be the device-GUI communication establishment. This is possible through an exchange of strings between the two entities and if the operation result is positive the connection between the GUI and the Device is obtained. At this point, the user should press the "Bridge Balancing" button to start the bridge balancing algorithm. This latter manages the read-out circuit based on the Wheatstone bridge with current control, its functioning is detailed in a further section, 5.1.1. The result of the balancing is printed on the Discovery Board LCD. If positive, it is possible to press the "Start" button and begin the signals acquisition. The acquired signals are the filtered and amplified ones, at the end of the signal conditioning chain. They are two, one for each channel and are sampled using channels 4 and 5 of the ADC peripherals. The ADC sampling rate is set to 1 Khz since it is triggered by an external timer interrupt generated every 1 ms. After every ADC conversion the sampled data are stored in a single output buffer that will be used to transmit them to the GUI. The buffer, whose structure is illustrated in figure 5.2, is 200-byte size with 100 16-bit cells, being two of the channel to be sampled. Every 1 ms its cells are filled with four bytes, two for each signal. The result is that every 50 ms the buffer is filled and can be sent to the GUI.

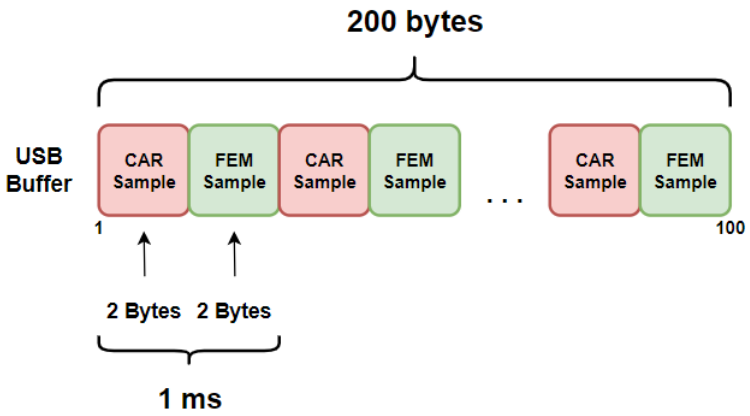

Figure 5.2: USB buffer structure illustartion.

Finally, whenever the user may decide to stop the signal acquisition it should press the "Stop" button. This will disable the timer and stop the ADC sampling.

A last aspect that the firmware handles is the possibility to check the buffer filling mechanism. This is useful in the case of signal acquisition issues to ensure and exclude the possibility of a buffer fill management trouble. To start this procedure, the user should press the "Debug" button enabling the setting of a to debug flag. Then, it is possible to start the signal acquisition, managed in the same manner as for the previous condition. However, in this case, the same 200-byte size buffer is filled with a software-generated ramp signal, called the "dummy signal". If there is no buffer filling errors the interface should display the ramp signal correctly increasing from 0 to 1000.

Listing 5.2: GUI commands handling.

```
48 char CMD_FROM_GUI[32] = { 0 };
49 extern volatile uint32_t acq_ongoing, init, cnt, debug;
50
51 void command_decode()
52 {
53     char buffer[32] = { 0 };
54
55     if (strncmp(CMD_FROM_GUI, "CMD", 3) == 0)
56     {
57         switch (CMD_FROM_GUI[3])
58         {
59             /* Who am I */
60             case '0':
61                 sprintf(buffer, "BIOPas01");
62                 while (is_USB_tx_busy(&USBD_Device)) {;}
63                 USBD_CDC_SetTxBuffer(&USBD_Device, (uint8_t*)&
    buffer, 8);
64                 if (USBD_CDC_TransmitPacket(&USBD_Device)!=
    USBD_OK)
65                 {
66                     TM_ILI9341_Puts(5, 70, "      USB comm. error
    2!    ", &TM_Font_11x18, ILI9341_COLOR_BLACK,
    ILI9341_COLOR_RED);
67                 }
68                 else
69                 {
70                     TM_ILI9341_Puts(5, 40, "      Device connected
        ", &TM_Font_11x18, ILI9341_COLOR_BLACK, ILI9341_COLOR_GRAY
    );
71                 }
72             break;
73
```

```
74              /* Start acquisition */
75              case '1':
76                  TM_ILI9341_Puts(5, 40, "      Acquisition ongoing
      ", &TM_Font_11x18, ILI9341_COLOR_BLACK, ILI9341_COLOR_GREEN
    );
77                  while (is_USB_tx_busy(&USBD_Device)) {;}
78                  acq_ongoing = 1;
79                  enable_TIM3_int();
80              break;
81
82              /* Stop acquisition */
83              case '2':
84                  TM_ILI9341_Puts(5, 40, "      Acquisition stopped
      ", &TM_Font_11x18, ILI9341_COLOR_BLACK, ILI9341_COLOR_RED);
85                  HAL_NVIC_DisableIRQ(TIM3_IRQn);
86                  acq_ongoing = 0;
87                cnt = 0;
88                init = 1;
89              break;
90
91              /* Bridge Balancing */
92              case '3':
93                  TM_ILI9341_Puts(5, 40, "      Calibration ongoing
      ", &TM_Font_11x18, ILI9341_COLOR_BLACK, ILI9341_COLOR_GREEN
    );
94                  InitBridge_CAR();
95                  InitBridge_FEM();
96              break;
97
98              /* System debug */
99              case '4':
100                 TM_ILI9341_Puts(5, 40, "        Debug ongoing
      ", &TM_Font_11x18, ILI9341_COLOR_BLACK, ILI9341_COLOR_GREEN)
    ;
101                 while (is_USB_tx_busy(&USBD_Device)) {;}
102                 acq_ongoing = 1;
103                 debug = 1;
104                 enable_TIM3_int();
105             break;
106
107             /* HW reset */
108             default:
109             HAL_NVIC_DisableIRQ(TIM3_IRQn);
110             acq_ongoing = 0;
111             cnt = 0;
112             init = 1;
113         }
114     }
115 }
```

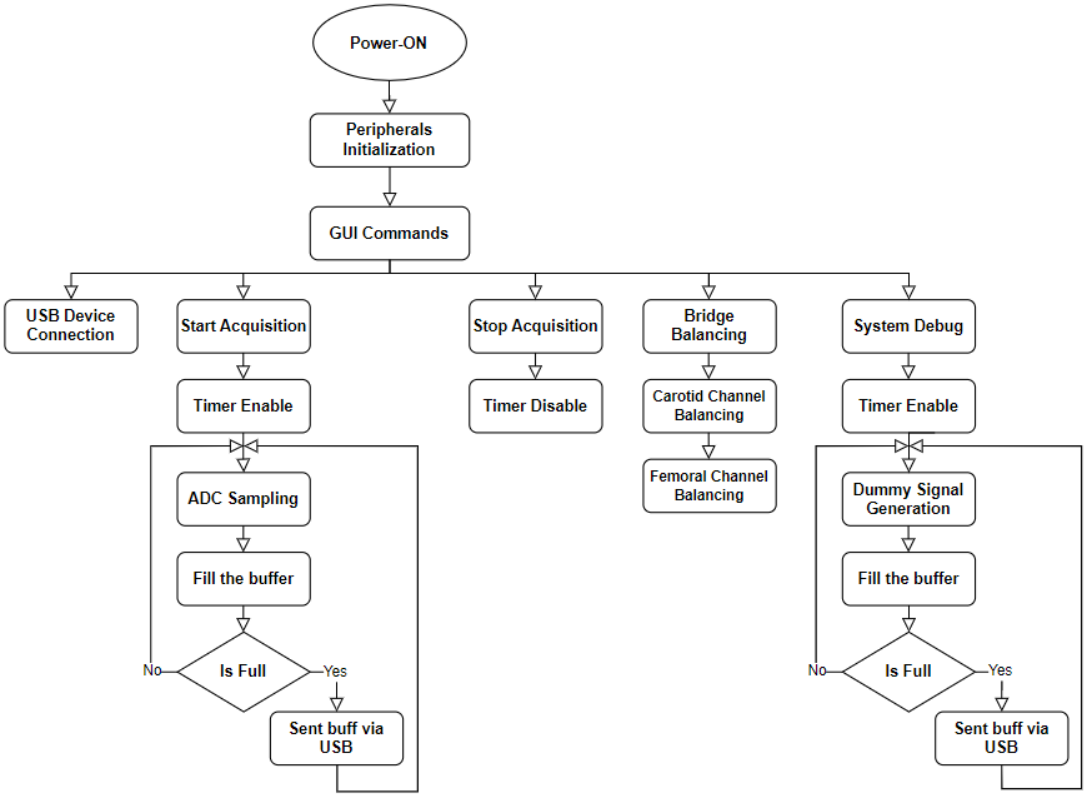

Figure 5.3: Firmware flow chart illustration.

5.1.1 Bridge Balancing Algorithm

As already detailed in the previous section the readout mechanism on which is based the system consists of a full-bridge Wheatstone configuration with current control. To provide its balancing, the branch's currents should be zeroed. Therefore, the starting point of this complex mechanism is the measurement of the current flowing from the two branches of the bridge to the transimpedance amplifiers inputs. To do so an INA333 is utilized, which amplifies the voltage falling on each sensing resistor. With the voltage, it is possible to extrapolate, by firmware, the correspondent current. The voltage reading is performed thanks to four ADCs channels, one for each bridge branch, configured in single shot mode and selected through the following channel selection function.

Listing 5.3: ADC1 channel configuration.

```
116 void configADC1_CH(uint32_t channel, uint8_t val)
117 {
118         ADC_ChannelConfTypeDef sConfig;
119 
120         sConfig.Channel = channel;
121         sConfig.SamplingTime = ADC_SAMPLETIME_3CYCLES;
122 
123         if(val == 1)
124         {
125           sConfig.Rank = 1;
126         }
127         else
128         {
129           sConfig.Rank = 0;
130         }
131 
132         HAL_ADC_ConfigChannel(&Adc1_Handle, &sConfig);
133 
134 }
```

The voltage sampling and the current extrapolation are the first step that the firmware executes. Following that, the firmware checks to determine whether the current is less than the set threshold. If this is the case, the branch is considered balanced, and the process ends. If not, it proceeds to test the current trend: if the current is decreasing compared to the previous check, V_{OFFSET} is decremented by 15mV, otherwise, V_{OFFSET} is incremented by 15mV. In both cases, the updated V_{OFFSET} is sent via SPI communication to the DAC, which converts the digital value into the corresponding analogue voltage and set it as one of the inputs of the transimpedance stage, forcing the other one to the same value. Once the optimal V_{OFFSET} is set, the firmware checks for others 50 times to ensure that the current value remains stable within the limit. Only when this condition is satisfied the branch is considered balanced, and the program passes to the next branches.

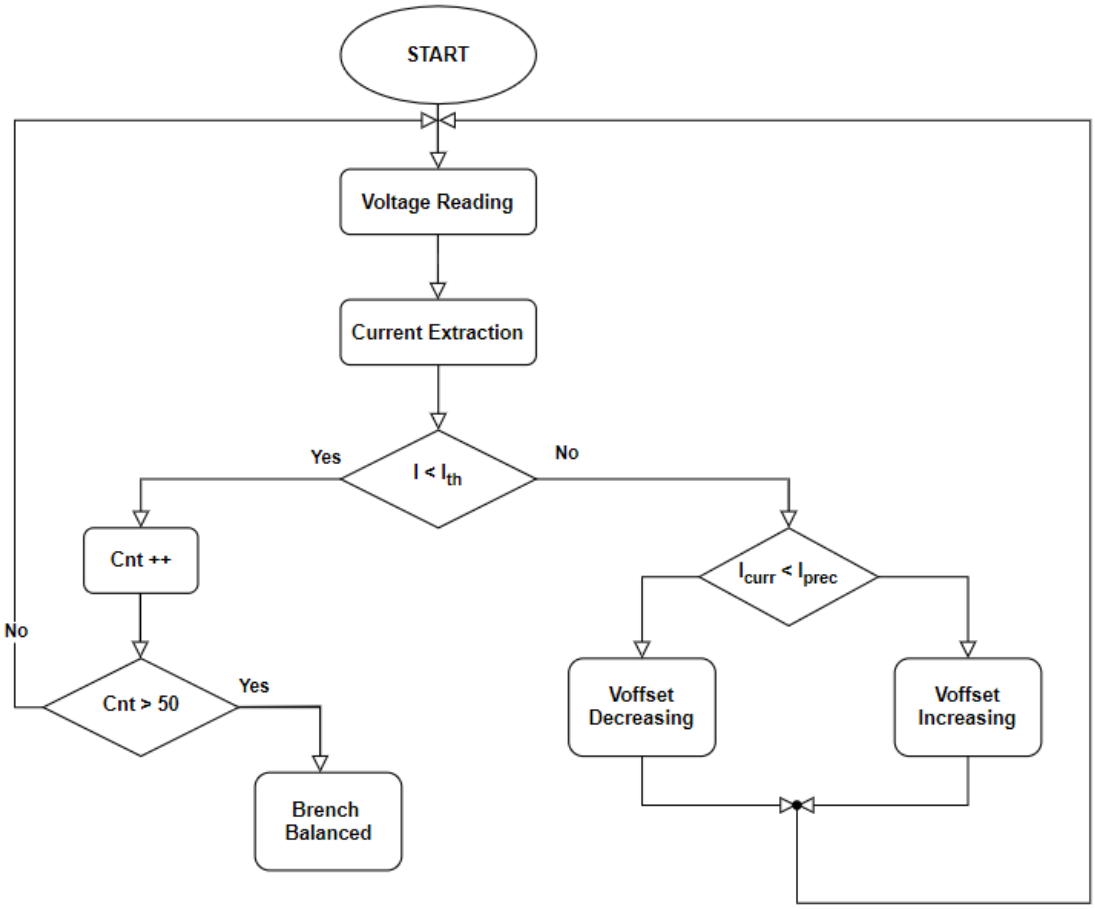

Figure 5.4: Bridge Balancing algorithm flowchart.

5.2 Graphical User Interface optimization

Another crucial aspect of the implemented system is the Graphical User Interface, which allows the user to easily interact with the device. Since the system is now based on an entirely different hardware, the GUI has needed to be redesigned. Starting form an already existing project, it has been adapted to this thesis application.

It has been developed in the Microsoft Visual Studio environment using C# and the declarative markup language XAML. The real-time signal display is the primary purpose of the GUI since it gives quick feedback on the quality of the acquired pulse waves. Since the signals from the femoral and carotid sites are collected simultaneously, there are two dedicated graphs on the interface. Furthermore, considering the purpose of the application, the GUI is provided with a a third graph where it is possible to display both the acquired pulse waves, overlapped. Finally, for further PWV parameter extraction, the GUI supports saving the information of the pulse waves, received on the laptop's VCOM.

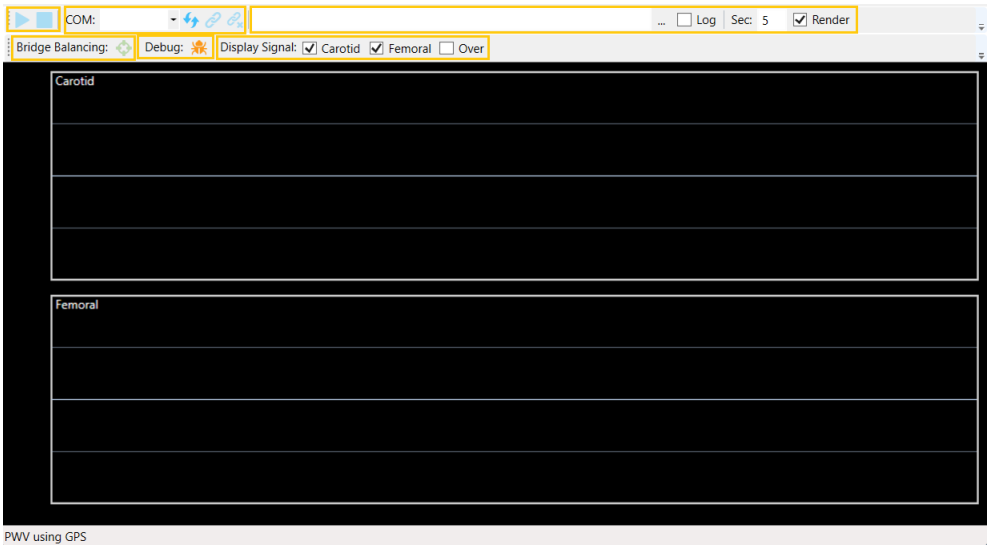

Figure 5.5: Graphical User Interface with a toolbar overview illustration.

The graphical toolbar is highlighted in figure 5.5. It is composed with several section in which dedicated buttons allows the user interaction and perform a specific task each:

– **Signal acquisition section**: includes the start and stop button useful for managing of the acquisition data process.

- **Device connection section**: includes a select box for selecting the COM and a connection/disconnection button to manage the connection with the device
- **Data savings section**: includes a text box in which the data file name should be defined and a check box to allow saving data in it.
- **Data display section**: includes three check box button for the selection of the signal to be displayed: carotid, femoral or their overlapping.
- **Bridge Balancing section**: is a single button that clicked starts the balancing algorithm.
- **System Debug section**: is a single button that clicked enables the generation of two dummy signal, one for each channel.

The starting point for the real time display of the pulse wave signal through the GUI is the creation of a Virtual COM port (VCOM). This is fundamental to establish the connection with the device and enabling the data transmission. The first step the user should perform by means of the appropriate buttons, is the choice of the COM and the connection with the device. Consequently, by pressing the "Bridge Balancing" button the firmware executes the balancing algorithm. Its outcome is printed on the LCD of the Discovery board and, if positive, the “Start” button on the interface become clear and available to be used. Indeed, at this point, the user can start the acquisition by pressing the correspondent button. In this way, via USB, the interface receives a data buffer of 200 bytes every 50 ms. To display data, this incoming buffer is unpacked and its content is reorganized into two separate buffer, one for each channel. The buffer reorganization mechanism and their structure is illustrated in the figure 5.6 below.

Another important function that the GUI provides is the possibility to verify whether the system is working properly or not, by checking if the interface buffer is properly filled. To do so, the user should press the "Debug" button that will trigger the generation of a "dummy signal" via firmware. By this way, the input buffer received via USB by the interface will be of the same size but will contains different informations.

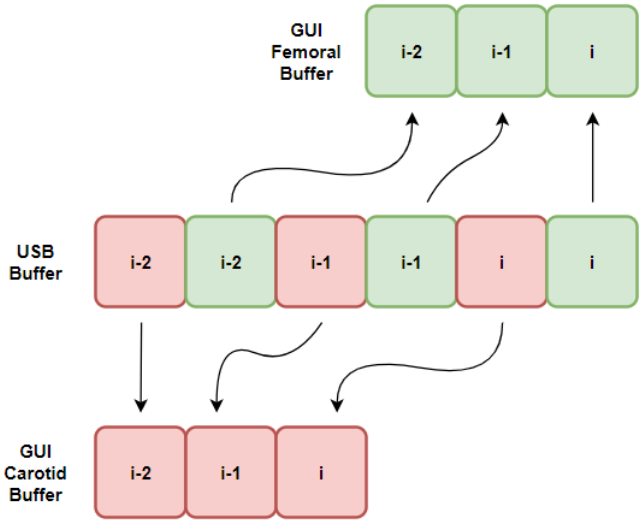

Figure 5.6: Graphical User Interface data reorganization.

Chapter 6

Result and discussion

This chapter is divided into two parts. In the first section, the complete final system architecture and the signal acquired through it are discussed. Then, in the second part, the tests carried out to investigate the possible reasons for the malfunction are detailed.

6.1 Signal acquisition

The final system architecture is shown in figure 6.1, consisting of the two sensing elements integrated directly with the peripheral PCBs and the microcontroller board (STM32 Discovery Kit) integrated with the Main PCB. The USB connection with the laptop allows for the real-time display of the acquired signal.

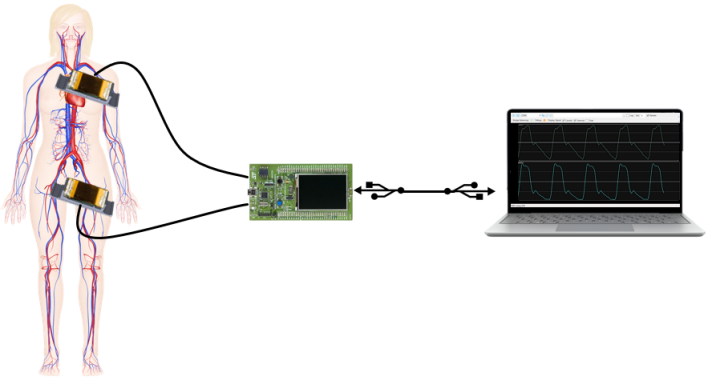

Figure 6.1: Final device configuration based on STM32Discovery Board.

Before considering the Pulse Wave signal acquisition, the system has been

tested to verify its capability of managing the acquisition from both channels. To do so, the ADCs channels have been fed with different signals such as sinusoidal, ramp or square waves, generated by instrumentation. In particular, the signal provided to one channel has been generated with the help of the 33220A functionarbitrary waveform generator from Agilent, while for the other channel, the signal has been generated through the digital oscilloscope Rigol MSO5072. This device integrates 7 independent instruments into 1, including one arbitrary waveform generator in a standard configuration of 2 waveform output channels for the hardware, capable of providing 13 predefined waveforms with up to 25 MHz frequency. Figure 6.2 shows the obtained results for the case of a triangular wave at 1 Hz generated for channel 1 (carotid) and a ramp signal at 1 Hz generated for channel 2(femoral). Furthermore, the two generated signals are provided with an offset voltage set to 1.5 V.

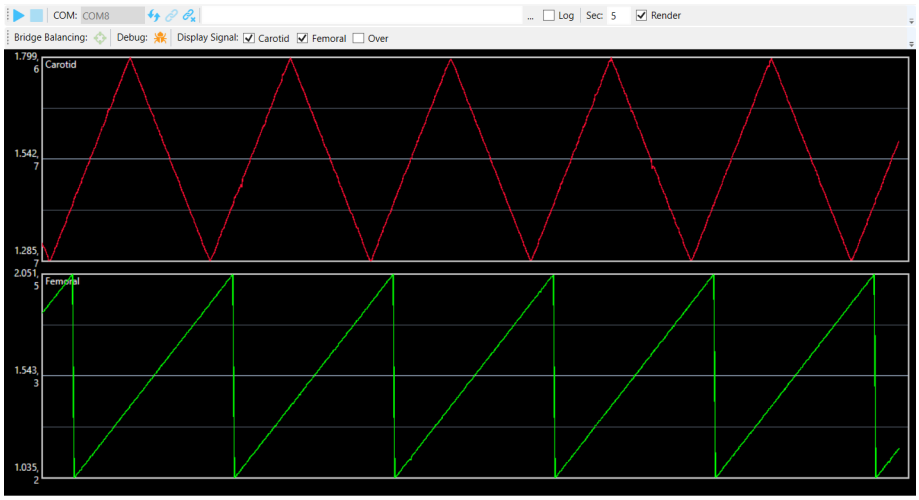

Figure 6.2: Real time display of the generated signal.

The result of this first step has been satisfactory demonstrating that the system is actually functioning. In particular, the ADCs channel configuration and the buffer is correctly filled for the real-time display of the acquired signals.

6.1.1 Rectangular configuration

Given the result of the previous test, the next step has been the integration of the graphene pressure sensors into the system, starting from the rectangular configuration. To check the signal acquisition the test has been carried out in the lab, thus in a non-clinical environment and without the help of a clinician's expert. During tests, different issues and possibly malfunctioning have been

discovered. Figure 6.3 illustrates the acquired signal on the Graphical User Interface. Starting from the carotid, despite the first pulse, the overall trend of the signal is very noisy and not satisfactory. In fact, even if the signal shows a periodicity its profile is not physiological. Even more so for the femoral channel. Despite its trend seeming to be less affected by the noise it shows a signal which is actually not a Pulse Wave.

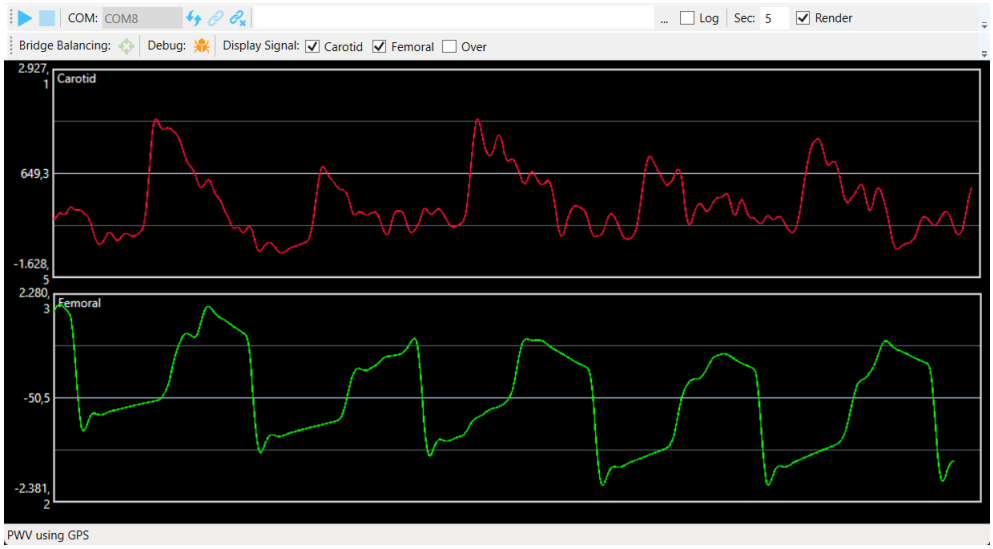

Figure 6.3: Real-time display of the last signal acquired with the rectangular configuration.

6.1.2 Circular configuration

Despite the problems encountered during the signal acquisition with the rectangular configuration it has been decided to continue testing the system with the circular sensors. To check the signal acquisition the test has been carried out with the same protocol in a non-clinical environment and without the help of a clinician's expert. The signal acquired through the circular cross section sensor is reported in figure 6.4. As for the previous configuration, the carotid signal shows a periodicity however the noise makes it impossible to be sure if indeed it is the pulse. The difference in terms of noise could be related to the system setup, where the circular case mounts a right angled header that very easily tends to move. Regarding the femoral instead, it has been impossible to detect a single pulse wave signal during the real time acquisition, as the signal shows a sinusoidal behaviour.

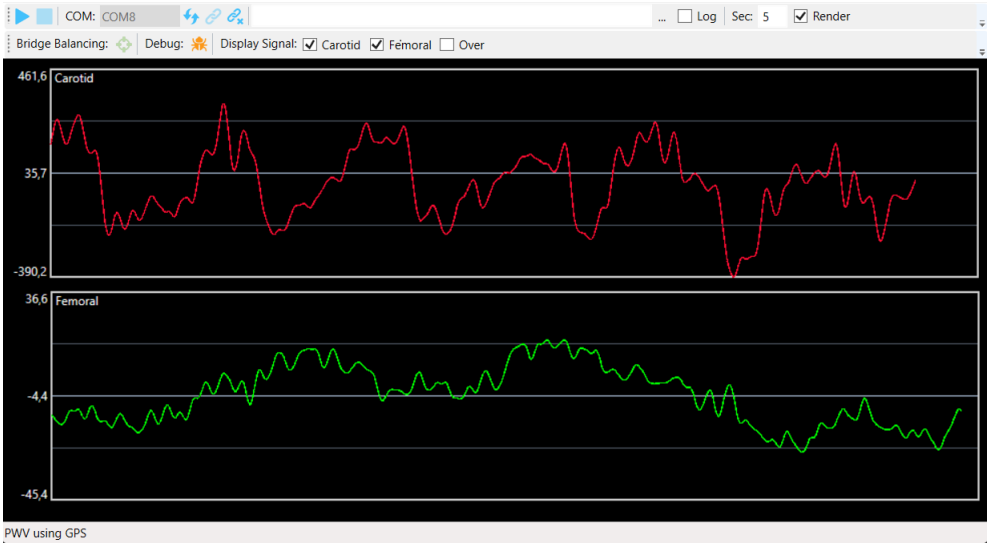

Figure 6.4: Real-time display of the last signal acquired with the circular configuration.

6.1.3 Matlab Analysis

To better investigate the signal behaviour the data acquired has been analyzed in Matlab. Starting from the rectangular configuration, the obtained curves are illustrated in figure 6.5. The signal acquired through the sensor at the carotid channel confirms its trend. It shows a single Pulse Wave but then start to be very noisy and no other useful information can be extracted. Concerning the femoral signal instead the trend seems to be less affected by noise and the periodicity is much more consistent. The analyzed data for the the circular configuration are shown in figure 6.6. Both carotid and femoral channel shows several peak however they seems to be much more affected by noise. In the end, it has been impossible to continue the validation process since a reliable Pulse Wave cannot be extracted. Based on these results, it has been decided to investigate the electronics. The step and the test followed are explained in the next section.

6.2 PCB testing

Given the results of the previous attempt at signal acquisition, a step back has been done. Starting from several analyses carried out during the signal acquisition to understand the possible source of malfunctioning, it has been decided to investigate the electronics.

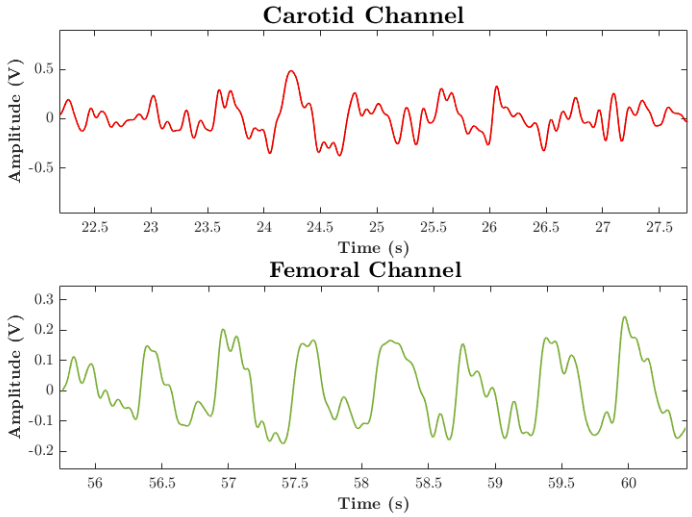

Figure 6.5: Rectangular configuration last signal analyzed on Matlab.

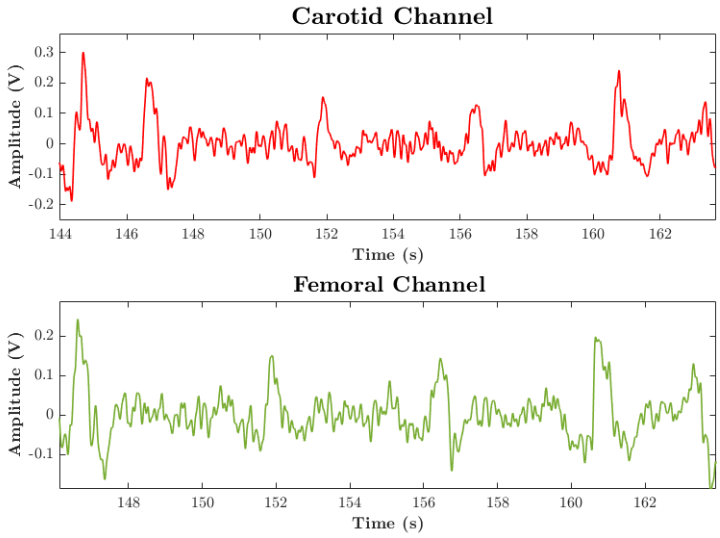

Figure 6.6: Circular configuration last signal analyzed on Matlab.

Specifically, the Printed Circuit Board has been inspected together with the components mounted on it, to check their behaviour.

6.2.1 DAC102S085 test

The test carried out on the DAC component concerns its correct initialization via firmware. As already discussed in section 4.4.2 the DAC102S085 is a DUAL

10-bit voltage-output digital-to-analog converter (DAC) that can operate from a single 2.7-V to 5.5-V supply. This component is a fundamental part of the conditioning circuit being responsible for the bridge nulling. In particular, it set the offset voltage at the output of the transimpedence stage necessary to zeros the current and get the Wheatstone bridge balanced. This voltage to be set is calculated via firmware and consequently updated via SPI. However, the tricky part is that the 16 input shift register of the DAC is provided with 12 data bits while the SPI sends the data into 8-bit frame. The developed solution is found on the `set_voffCAR()` function, nevertheless to check whether the component is correctly controlled (and functioning) the following function has been developed to set its output voltages to 1.65 V.

Listing 6.1: DAC voltage output controll.

```
135 void setDAC()
136 {
137     uint16_t value_DAC;
138     float voffset = 1.65;
139 
140     value_DAC = 1023;
141     upperdata1 = (value_DAC>>6) | 32;
142     lower1 = (uint8_t)(value_DAC<<2);
143     lowerdata1 =(uint8_t)lower1;
144 
145     HAL_GPIO_WritePin(GPIOD, GPIO_PIN_7, GPIO_PIN_RESET);
146     SPI_Send(SPI3,upperdata1);
147     SPI_Send(SPI3,lowerdata1);
148     HAL_GPIO_WritePin(GPIOD, GPIO_PIN_7, GPIO_PIN_SET);
149 
150 }
```

Finally, to check the correspondence of the values on the hardware, the PCB has been inspected by measuring the voltage values on every pin of the component with the tester. The obtained results were:

PIN		**TYPE**	**MEASURED VOLTAGE (V)**
N.	**NAME**		
1	V_a	Supply	3,2 V
2	V_{outa}	Analog Output	1,56 V
3	V_{outb}	Analog Output	1,56 V
4,5	NC	-	0 V
6	GND	Ground	0 V
7	V_{ref}	Analog Input	1,56 V

Table 6.1: DAC102S08 inspected voltage values on the rectangular PCB.

The result of these tests has been positive demonstrating that the control of the DAC102S085 via firmware is successful. The only thing to note is the value on the analog input pin V_{ref}, which is 70 mV lower than the expected reference voltage value of 1.65 V. According to the DAC output voltage equation, V_{out} is directly proportional to V_{ref}. This latter is an analog voltage that depends only on the physical circuit and cannot be controlled by firmware. Therefore, a further investigation in this direction has been executed.

6.2.2 Voltage reference test

Through the help of the tester, the voltage reference block on the two peripheral PBCs has been inspected.

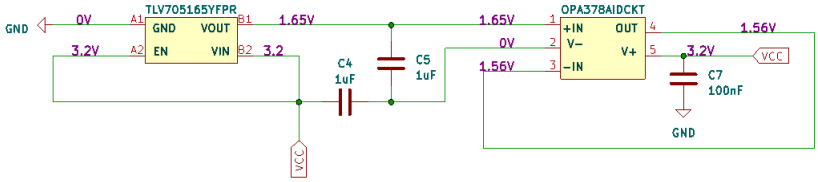

Figure 6.7: Voltage values measured on the Carotid PCB.

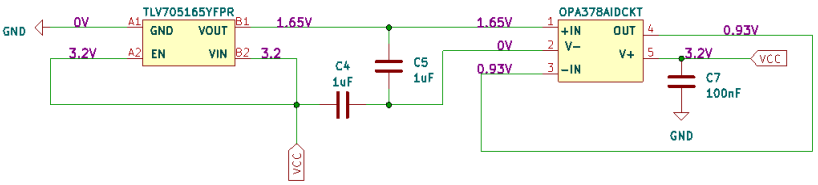

Figure 6.8: Voltage values measured on the Femoral PCB.

The measured values are given in the figures. For both channels the voltage regulator TLV705 component seems to work properly but then, proceeding with testing, some issues were identified. Considering the Carotid PBCs only, the output pin 4 of the OPA378 is giving a 1.56V voltage values, which is exactly the value found at the Analog Input Pin 7 of the DAC. However, this is quite peculiar since the OPA378 main function is to output buffer. Ones should expect to have on its Output Pin 4 the same voltage as the input: 1,65V. Proceeding testing the other channel, the femoral Rectangular PCBs, the output pin 4 of the OPA378 is giving 0.93V which is far from what expected. In conclusion, these tests have brought to light a not correct behaviour for both Carotid and Femoral rectangular PCBs which must be

further investigated to better understand the issues and provide the correct reference voltage to the whole circuit.

6.2.3 INA333 test

Continuing to test the signal conditioning chain, the next fundamental component under analysis is the INA333 of the rectangular peripheral PCB. This element is responsible for the amplification of the small voltage signal coming from the transimpedence stage therefore its possible malfunctioning may affect the signal acquisition. The test carried out has followed the same procedure as for the DAC, using the digital multimeter to check for the voltage values on the PCB. However, on the basis of the previous results this test has been executed only on the "functioning" rectangular PCB, the carotid. Given the measured values, considering that the gain resistance is R_g=1.1 KΩ and the correspondent gain is G=100 the amplified output voltage results to be:

$$V_{OUT} = (V_+ - V_-)G = (0.33 - 0.31)100 = 2.1V \tag{6.1}$$

The result of this test were positive revealing that the Instrumentation Amplifier is actually capable to correctly amplify the input voltage difference.

6.2.4 Programmable Gain Amplifier test

The final step has been the test of the Main PCB. In this case, the fundamental block is the PGA which is responsible for the final amplification of the filtered signal coming from the rectangular pheripheral PCBs. Since this device is obtained with the INA333 for the signal amplification and a CMOS digital switch, the MAX4781, for the selection of the gain resistance, both elements have been inspected on the Printed Circuit Board. The test, carried out on both Carotid and Femoral channels, consist of gradually changing the gain resistance of the INA333 to check whether the output voltage amplification increases or not. The gain is controlled via firmware by setting the pin state of the correspondent configured GPIOs 4.2, and the different values are changed according to the resistance selected, as already detailed in table 4.1.

The **first step** of the test involves the digital multiplexer, to check whether the switch are correctly programmed by the firmware and the corresponding resistance value is set. Starting from the truth table provided by its datasheet, the GPIOs state has been configured via software and than, to verify the result of these operation the PCB has been inspected. The obtained analog voltage values measured with the help of the tester are listed in table 6.2 and 6.3.

LOGIC LEVEL			**MEASURED V (V)**			**SELECTED R_g (Ω)**
C	**B**	**A**	**C**	**B**	**A**	
L	L	L	0	0.2	0	2040
L	L	H	0	0.1	2.8	1000
L	H	L	0	0.1	0	560
L	H	H	0	0.1	2.8	400
H	L	L	2.8	0.1	0	300
H	L	H	2.8	0.1	2.8	220
H	H	L	2.8	2.8	0	130
H	H	H	2.8	0.1	2.8	100

Table 6.2: Analog voltage values measured at the input of the carotid MAX4781 digital switch.

LOGIC LEVEL			**MEASURED V (V)**			**SELECTED R_g (Ω)**
C	**B**	**A**	**C**	**B**	**A**	
L	L	L	0	0	0	2040
L	L	H	0	0	2.8	1000
L	H	L	0	2.8	0	560
L	H	H	0	2.8	2.8	400
H	L	L	2.8	0	0	300
H	L	H	2.8	0	2.8	220
H	H	L	2.8	2.8	0	130
H	H	H	2.8	2.8	2.8	100

Table 6.3: Analog voltage values measured at the input of the femoral MAX4781 digital switch.

The logic level column report the state that each input pin should have to select the correct switch while the measured voltage column shows the value obtained with the tester. Overall, the results of this simple test shows the analog multiplexer is working properly and the firmware is capable to correctly control the component. One thing to note concerns the input B of the carotid channel. Unlike the other, it shows unexpected voltage values for both low or high logic state of the pin.

Nevertheless it has been decided to continue with the **second step** of the test which concerns the INA333, to check if it is correctly amplifying its input voltage difference. The procedure followed consist in gradually set, via firmware, each of the 7 possible value of the gain and then measure on the PCB the output voltage of the Instrumentation Amplifier. The obtained voltage

values have been plotted on Matlab and are shown in 6.9, 6.10.

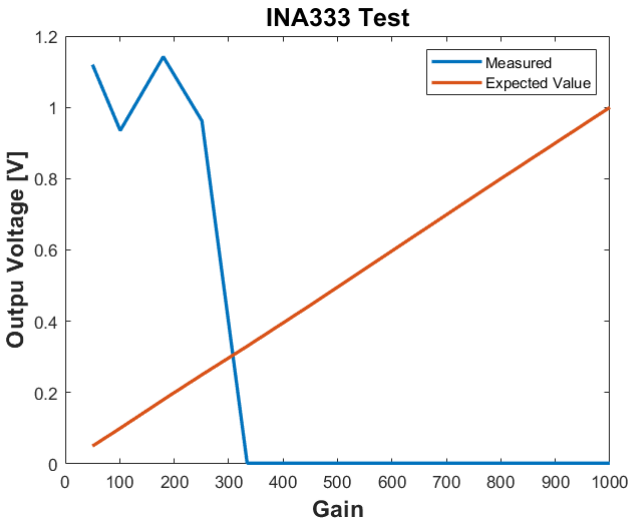

Figure 6.9: INA333 output voltage values measured on the Carotid PCB.

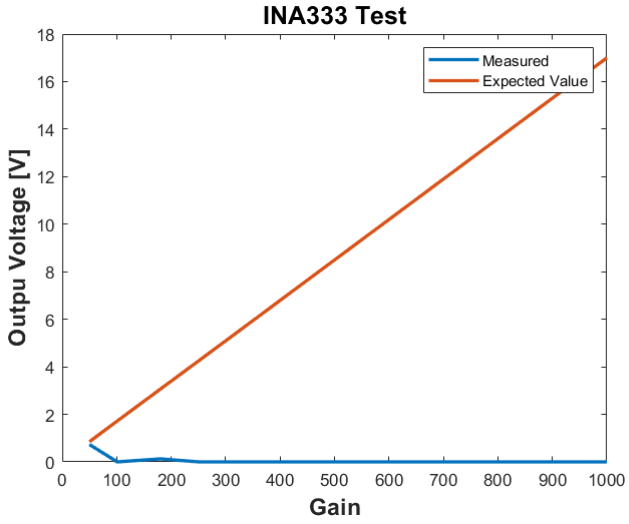

Figure 6.10: INA333 output voltage values measured on the Femoral PCB.

Concerning the Carotid channel is noticeable how none of the output voltage values are actually the expected. Furthermore they assumes values which do not correspond to the input difference amplified. By gradually decreasing the resistance Rg values the gain increases and the same should be for the voltage but this is not the case, the trend seems to be the opposite, since it

decreases for increasing gains. As a result, the carotid channel final stage of amplification is not working properly and further investigation on the possible source of error must be done.

Concerning the Femoral channel the result are not so different. The voltage values measured on the PCB do not coincide with the expected amplification and are completely out of range. In addition, for this channel, in the majority of the cases the measured voltage is zero. As a result, the femoral channel final stage of amplification is not working. However, in this case, it was expected considering the issues discovered in section 6.1.

The outcome of these test revealed a not correct amplification at the final stage of the conditioning circuit that influences the signal acquisition and thus must be investigated in detail.

6.2.5 Conclusion

The electrical evaluation conducted on the Printed Circuit Board have brought to light important malfunctioning that surely affects the signal acquisition. Furthermore, the detected sensor degradation phenomena contributes to the quality of the acquired signal making impossible to correctly asses the Pulse Wave signal.

Chapter 7

Conclusions and future work

The aim of this thesis was the optimization of the already designed at the experimental stage, Pulse Wave Velocity estimation system based on innovative graphene pressure sensors. This non-invasive and low-cost device consist of a conditioning circuit integrated on two different PCBs and a Pyboard D-series to manage the signal acquisition and the USB communication with a laptop. Furthermore, a graphical user interface (GUI) enables the interaction with the device by changing the gain, plotting data in real-time and saving them in text files. The sensing elements are innovative graphene pressure sensors developed by the Nanochemistry group at the "Institut de Science et d'Ingénierie Supramoléculaires" of the University of Strasbourg. They were fabricated, at non-industrial level, into two shape: rectangular and circular. Furthermore they represent a new generation of graphene pressure sensor thus it has been fundamental the understanding of their sensibility.
The starting point of the thesis work has been their characterization to identify the best functioning and replace it into the system. Starting from the obtained baseline resistances, the best functioning have been selected and integrated into the system. After that, it has been necessary an optimization for the sensors supports which should be able to hold the new "sensor-PCBs" unit. The result of the design has been two new supports, one characterized by a rectangular shape suitable for the rectangular sensor and the other with a pen-shape suitable for the integration of the circular ones.
At this point, to consolidate the validation process, the system in its new optimized configuration, has been tested in a clinical environment. The trial has been carried out with the help of a clinician in collaboration with "A.O.U.

Città della Salute e della Scienza di Torino" and despite the different setup tested, both circular and rectangular sensor gave unsatisfactory results. Specifically, the system were able to acquire the Pulse Wave but the stability and reliability needed for the application were insufficient.
Considering the issues to be mainly electronic the Pyboard D-Series has been replaced with the STM32 Discovery kit. A new firmware has been developed, capable to manage different aspects simultaneously such as the Wheatstone bridge balancing, the real-time signal display on the GUI or the system debug. In addition, the conditioning circuit has been maintained but, to adapt it with the new hardware, a new Printed Circuit Board (PCB) has been designed. It has been conceived in a "shield" configuration to be integrated directly with the Discovery board and reduce possible electrical noise.
This final system configuration based on a different microcontroller has been integrated with the rectangular pressure sensor and than, it has been tested in a non clinical environment. The result of the signal acquisition were poor and the Pulse Wave Waveform impossible to be detected. Further test involved the circular sensor however the results have been worse.
Given that, the final part of the thesis work involved the inspection of the electronics. Starting from the peripheral PCBs each component of the conditioning circuit has been tested. Concerning the peripheral PCB the results show a correct functioning of both the Digital-to-Analog Converter responsible for the offset setting and the Instrumentation Amplifier useful for the signal amplification. However, it was determined that the voltage reference stage is unable to set the appropriate 1.65V voltage value, which explains why the acquired signal is not centered to the reference. Further inspection on the Main PCB have brought to light important malfunctioning regarding the Programmable Gain Amplifier that surely affects the signal acquisition and its correct real-time visualization on the GUI. A final test involves the sensing element, for which has been found an increased baseline resistance value that makes the conditioning circuit unsuitable.
In conclusion, the detected electronic problems combined with the sensor deterioration phenomena have made it impossible to proceed with validations and therefore acquire reliable results. In future, a first aspect to be investigate in-depth is the pressure sensor deterioration phenomena together with the possible solution to make them more stable. Furthermore, focusing on the electronics, it is important to correct the detected malfunctions and, in the perspective of developing a portable device, a optimized Main PCB can be designed focusing on the integration of the STM32F429ZI MCU and the ST-LINK/V2 module.

Bibliography

[1] Anatomy of the Cardiovascular System. «MCAT Biology Review». In: (). URL: https://schoolbag.info/biology/mcat/32.html (cit. on p. 4).

[2] Cardiology Associates of Michigan. «Basic Anatomy of the Human Heart». In: (). URL: https://www.cardofmich.com (cit. on p. 5).

[3] Lambros S Athanasiou, Dimitrios I Fotiadis, and Lampros K Michalis. *Atherosclerotic plaque characterization methods based on coronary imaging*. Academic Press, 2017 (cit. on p. 6).

[4] Mohan Satish and Prasanna Tadi. «Physiology, vascular». In: *StatPearls [Internet]*. StatPearls Publishing, 2022 (cit. on p. 7).

[5] Goksel Guven, Matthias P Hilty, and Can Ince. «Microcirculation: physiology, pathophysiology, and clinical application». In: *Blood Purification* 49.1-2 (2020), pp. 143–150 (cit. on p. 9).

[6] Anna Chruscik, Kate Kauter, Louisa Windus, Eliza Whiteside, and Leanne Dooley. «Fundamentals of anatomy and physiology». In: (2021) (cit. on pp. 10, 14).

[7] Robert S. Schwartz. *Blood*. Jan. 2023. URL: https://www.britannica.com/science/blood-biochemistry (cit. on p. 11).

[8] Francis L Belloni. «Teaching the principles of hemodynamics.» In: *Advances in Physiology education* 277.6 (1999), S187 (cit. on p. 12).

[9] Lung National Heart and Blood Institute. *Framingham Heart Study (FHS)*. URL: https://www.nhlbi.nih.gov/science/framingham-heart-study-fhs (cit. on p. 14).

[10] Koon K Teo and Talha Rafiq. «Cardiovascular risk factors and prevention: a perspective from developing countries». In: *Canadian Journal of Cardiology* 37.5 (2021), pp. 733–743 (cit. on p. 15).

[11] Maxwell Birger, Alexander S Kaldjian, Gregory A Roth, Andrew E Moran, Joseph L Dieleman, and Brandon K Bellows. «Spending on cardiovascular disease and cardiovascular risk factors in the United States: 1996 to 2016». In: *Circulation* 144.4 (2021), pp. 271–282 (cit. on p. 15).

[12] Felicitas E Hengel, Christian Sommer, and Ulrich Wenzel. «Arterial Hypertension». In: *Deutsche Medizinische Wochenschrift (1946)* 147.7 (2022), pp. 414–428 (cit. on p. 16).

[13] Julio A Chirinos, Patrick Segers, Timothy Hughes, and Raymond Townsend. «Large-artery stiffness in health and disease: JACC state-of-the-art review». In: *Journal of the American College of Cardiology* 74.9 (2019), pp. 1237–1263 (cit. on p. 16).

[14] Yi Zhang, Patrick Lacolley, Athanase D Protogerou, and Michel E Safar. «Arterial stiffness in hypertension and function of large arteries». In: *American Journal of Hypertension* 33.4 (2020), pp. 291–296 (cit. on pp. 16, 17).

[15] John F Moran. «Pulse». In: *Clinical Methods: The History, Physical, and Laboratory Examinations. 3rd edition* (1990) (cit. on pp. 17, 19).

[16] Stephen A Esper and Michael R Pinsky. «Arterial waveform analysis». In: *Best Practice & Research Clinical Anaesthesiology* 28.4 (2014), pp. 363–380 (cit. on p. 18).

[17] John F Butterworth IV, David C Mackey, and John D Wasnick. «Morgan & Mikhail's». In: (2013) (cit. on p. 20).

[18] Julio A Chirinos, Patrick Segers, Timothy Hughes, and Raymond Townsend. «Large-artery stiffness in health and disease: JACC state-of-the-art review». In: *Journal of the American College of Cardiology* 74.9 (2019), pp. 1237–1263 (cit. on p. 20).

[19] Giorgia Fiori, Fabio Fuiano, Andrea Scorza, Silvia Conforto, and Salvatore Andrea Sciuto. «Non-invasive methods for PWV measurement in blood vessel stiffness assessment». In: *IEEE Reviews in Biomedical Engineering* (2021) (cit. on pp. 20–22).

[20] DiaTecne. *PulsePen*. URL: `https://www.pulsepen.com/pulsepen.html` (cit. on p. 23).

[21] Alam Medical. *Complior Analyse*. URL: `http://www.complior.com/products` (cit. on p. 23).

[22] AtCor. *SphygmoCor Platform*. URL: `https://atcormedical.com/technology/sphygmocor-xcel/` (cit. on p. 23).

[23] Irene Buraioli, Davide Lena, Alessandro Sanginario, Dario Leone, Giulia Mingrone, Alberto Milan, and Danilo Demarchi. «A new noninvasive system for clinical pulse wave velocity assessment: The Athos device». In: *IEEE Transactions on Biomedical Circuits and Systems* 15.1 (2021), pp. 133–142 (cit. on p. 23).

[24] American Society of Hematology. *Hematology Glossary*. URL: `https://www.hematology.org/education/patients/blood-basics`.

[25] European Society of Cardiology. *EU Action on CVD*. URL: `https://ehnheart.org/eu-action-on-cvd.html`.

[26] S Magder. «The meaning of blood pressure». In: *Critical Care* 22.1 (2018), pp. 1–10.

[27] Joshua D Pollock, Ian Murray, Stephen Bordes, and Amgad N Makaryus. «Physiology, cardiovascular hemodynamics». In: (2017).

[28] Pierre Boutouyrie, Phil Chowienczyk, Jay D Humphrey, and Gary F Mitchell. «Arterial stiffness and cardiovascular risk in hypertension». In: *Circulation research* 128.7 (2021), pp. 864–886.

[29] William L. Winters. *hypertension*. Dec. 2022. URL: `https://www.britannica.com/science/hypertension`.

[30] John F Moran. «Pulse». In: *Clinical Methods: The History, Physical, and Laboratory Examinations. 3rd edition* (1990).

[31] Reference Values for Arterial Stiffness' Collaboration. «Determinants of pulse wave velocity in healthy people and in the presence of cardiovascular risk factors:'establishing normal and reference values'». In: *European heart journal* 31.19 (2010), pp. 2338–2350.

[32] P Salvi, E Magnani, F Valbusa, D Agnoletti, C Alecu, L Joly, and A Benetos. «Comparative study of methodologies for pulse wave velocity estimation». In: *Journal of human hypertension* 22.10 (2008), pp. 669–677.

[33] Giorgia Fiori, Fabio Fuiano, Andrea Scorza, Silvia Conforto, and Salvatore Andrea Sciuto. «Non-invasive methods for PWV measurement in blood vessel stiffness assessment». In: *IEEE Reviews in Biomedical Engineering* (2021).

[34] MZ Ansari and BS Gangadhara. «Piezoresistivity and its applications in nanomechanical sensors». In: *Procedia Materials Science* 5 (2014), pp. 1308–1313.

[35] Chang Bo Huang, Samanta Witomska, Alessandro Aliprandi, Marc Antoine Stoeckel, Massimo Bonini, Artur Ciesielski, and Paolo Samorì. «Molecule–Graphene Hybrid Materials with Tunable Mechanoresponse: Highly Sensitive Pressure Sensors for Health Monitoring». In: *Advanced Materials* 31 (2019) (cit. on pp. 26, 27).

[36] Qingbin Zheng, Jeng-hun Lee, Xi Shen, Xiaodong Chen, and Jang-Kyo Kim. «Graphene-based wearable piezoresistive physical sensors». In: *Materials Today* 36 (2020), pp. 158–179.

[37] Shou-En Zhu, Murali Krishna Ghatkesar, Chao Zhang, and GCAM Janssen. «Graphene based piezoresistive pressure sensor». In: *Applied Physics Letters* 102.16 (2013), p. 161904.

[38] Farid Sayar Irani, Ali Hosseinpour Shafaghi, Melih Can Tasdelen, Tugce Delipinar, Ceyda Elcin Kaya, Guney Guven Yapici, and Murat Kaya Yapici. «Graphene as a piezoresistive material in strain sensing applications». In: *Micromachines* (2022).

[39] C. Huang, S. Witomska, A. Aliprandi, M. Stoeckel, M. Bonini, A. Ciesielski, and Paolo Samorı. «Molecule–graphene hybrid materials with tunable mechanoresponse: highly sensitive pressure sensors for health monitoring». In: *Advanced materials* (2019).

[40] A. De Marcellis, G. Ferri, and P. Mantenuto. «Analog Wheatstone bridge-based automatic interface for grounded and floating wide-range resistive sensors». In: *Sensors and Actuators B: Chemical* (2013) (cit. on p. 38).

[41] A. Rosato and S. Torre. «Development of a clinical Pulse Wave Velocity estimation system using innovative graphene pressure sensors». PhD thesis. Politecnico di Torino, 2021 (cit. on p. 39).

[42] *Pyboard D-series references*. URL: `https://pybd.io/hw/pybd_sfxw.html` (cit. on pp. 43, 44).

[43] *STM32F722xx/ STM32F723xx*. URL: `https://www.st.com/resource/en/datasheet/stm32f723ze.pdf`.

[44] Texas Instrument. *TLV705 200-mA, Low IQ, Low-Noise, Low-Dropout Regulator in Ultra-Small, 0.77-mm × 0.77-mm DSBGA and PicoStarTM.* 2017.

[45] Onsemi. *Voltage Regulator NCV8114 - CMOS, Low Dropout 300 mA*. 2016 (cit. on p. 49).

[46] Texas Instrument. *MicroPower, Rail-to-Rail Operational Amplifiers. OPA347, OPA2347, OPA4347.* 2007 (cit. on p. 41).

[47] Texas Instrument. *Low-Noise, 900kHz, RRIO, Precision Operational Amplifier Zero-Drift Series. OPA378, OPA2378*. 2009.

[48] Texas Instrument. *DAC102S08510-Bit Micro Power DUAL Digital-to-Analog Converter With Rail-to-Rail Output*. 2016 (cit. on pp. 41, 52).

[49] Texas Instrument. *INA333 Micro-Power (50A), Zerø-Drift, Rail-to-Rail Out Instrumentation Amplifier. INA333*. 2015.

[50] Maxim Integrated Products. *High-Speed, Low-Voltage, 0.7CMOS AnalogSwitch┤es/Multiplexers. MAX4781 MAX4782 MAX4783*. 2005.

[51] *RM0090 Reference manual, STM32F429/439 advanced Arm®-based 32-bit MCUs*. 2021. URL: http://www.st.com (cit. on p. 51).

[52] *UM1662 User manual*. URL: www.st.com/stm32f4-discovery. (cit. on p. 50).

[53] *Rigol MSO5000 Series Digital Oscilloscope*. URL: https://asset.conrad.com/media10/add/160267/c1/-/en/001883450DS00/scheda-tecnica-1883461-rigol-mso5072-oscilloscopio-digitale-70-mhz-8-gsas-100-mpts-8-bit-1-pz.pdf..